iScience

CellPress
OPEN ACCESS

Article

Single-cell RNA-seq analysis reveals dual sensing of HIV-1 in blood Axl^{+} dendritic cells

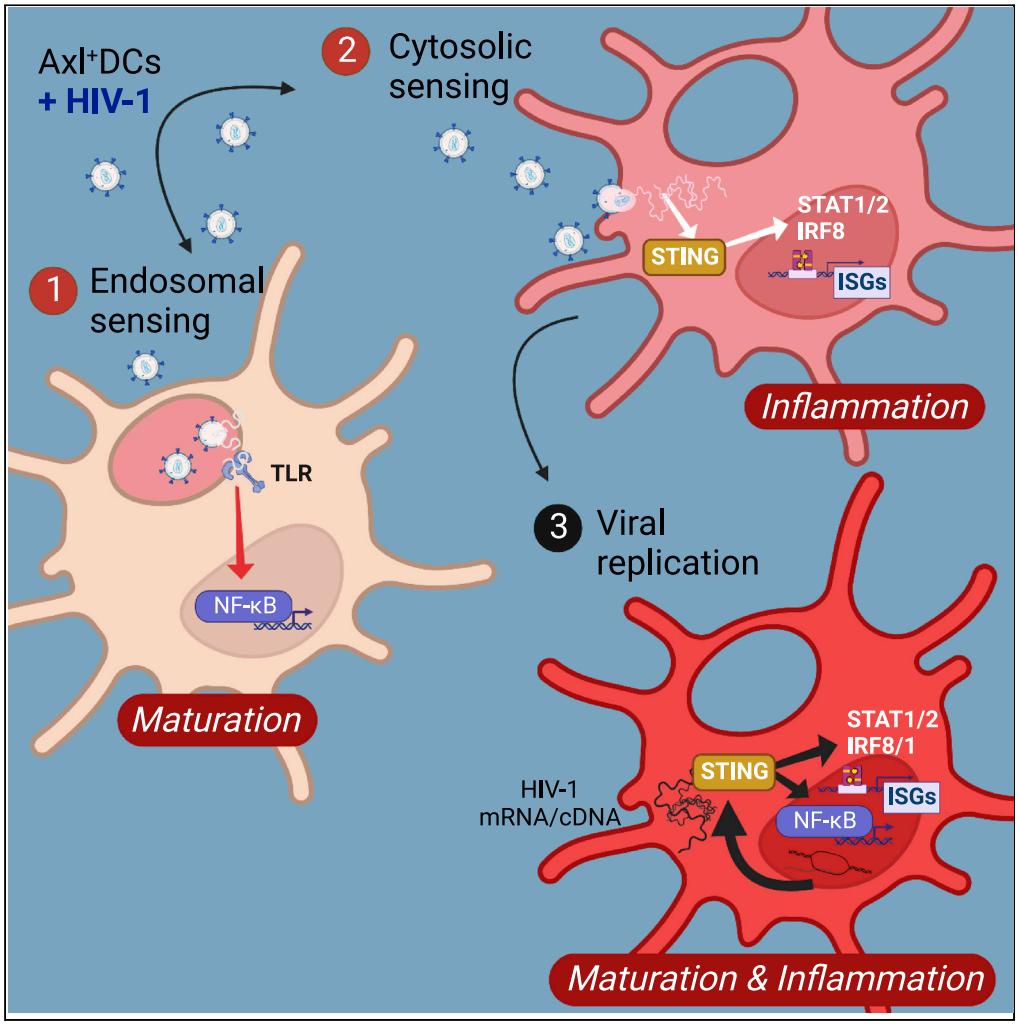

Flavien Brouiller, Francesca Nadalin, Pierre-Emmanuel Bonté, ..., Florent Ginhoux, Nicolas Ruffin, Philippe Benaroch

nicolas.ruffin@ki.se (N.R.)
philippe.benaroch@curie.fr (P.B.)

Highlights

Axl^{+}DCs are unique among human blood DC subsets in their response to HIV-1

HIV-1 induces 2 transcriptional programs in Axl^{+}DCs, likely through different sensors

The NF-KB-mediated program is RT-independent and activates T cell help functions

The STA1/2 program induces type I IFN and ISG responses through STING activation

Brouiller et al., iScience *26*, 106019
February 17, 2023
https://doi.org/10.1016/j.isci.2023.106019

iScience

CellPress
OPEN ACCESS

Article

Single-cell RNA-seq analysis reveals dual sensing of HIV-1 in blood Axl$^+$ dendritic cells

Flavien Brouiller,[1,8] Francesca Nadalin,[1,8] Pierre-Emmanuel Bonté,[1,8] Ouardia Ait-Mohamed,[1] Constance Delaugerre,[2,3] Jean-Daniel Lelièvre,[4] Florent Ginhoux,[5,6,7] Nicolas Ruffin,[1,9,10,*] and Philippe Benaroch[1,9,11,*]

SUMMARY

Sensing of incoming viruses is a pivotal task of dendritic cells (DCs). Human primary blood DCs encompass various subsets that are diverse in their susceptibility and response to HIV-1. The recent identification of the blood Axl$^+$DC subset, endowed with unique capacities to bind, replicate, and transmit HIV-1 prompted us to evaluate its anti-viral response. We demonstrate that HIV-1 induced two main broad and intense transcriptional programs in different Axl$^+$DCs potentially induced by different sensors; an NF-κB-mediated program that led to DC maturation and efficient CD4$^+$ T cell activation, and a program mediated by STAT1/2 that activated type I IFN and ISG responses. These responses were absent from cDC2 exposed to HIV-1 except when viral replication was allowed. Finally, Axl$^+$DCs actively replicating HIV-1 identified by quantification of viral transcripts exhibited a mixed NF-κB/ISG innate response. Our results suggest that the route of HIV-1 entry may dictate different innate sensing pathways by DCs.

INTRODUCTION

Dendritic cells (DCs) are crucial for pathogen recognition and the initiation of adaptive immune responses.[1] In addition, DCs are thought to be important for establishing and disseminating HIV-1 in the host and thus play a role in anti-viral immunity and HIV-1 transmission.[2] At the mucosal site, where immune cells first encounter HIV-1, various DC populations are present.[3] Among them, Langerhans cells and cervical CD14$^+$CD11$^+$ myeloid cells can capture and transmit HIV-1 to CD4$^+$ T cells, the former being also susceptible to HIV-1 infection.[4–6] Yet, how the various primary human DCs detect and respond to HIV-1 remains poorly understood.

Functional studies using tissue-derived DCs are difficult to perform because of their scarcity and the deleterious impact of isolation techniques they require.[3] Thus, most of the studies on HIV-1 innate sensing by DCs have been performed using *in vitro* differentiated DCs,[7] and only a few studies have been performed with fresh primary human DCs.[8–11] Early studies on monocyte-derived DCs (MDDCs) demonstrated that HIV-1 retrotranscription is necessary to induce cell maturation, as judged by the expression of the co-stimulatory molecule CD86.[12] However, HIV-1 replication in myeloid cells is highly restricted by the SAMHD1 enzyme that degrades the cytosolic pool of dNTP but is counteracted by HIV-2 coded protein Vpx.[13–16] Co-culture of monocyte-derived DCs (MDDCs) with autologous CD4$^+$ T cells down-regulated SAMHD1, leading to increased HIV-1 replication and sensing in DCs, suggesting that DC-lymphocyte cross-talk could result in viral replication in DCs *in vivo*.[17] Insight into the signaling pathways involved in MDDC exposed to HIV-1 in the presence of Vpx, led to the identification of the cGAS–STING pathway entailed in the induction of an interferon (IFN) response and DC maturation.[12,18,19] Whether similar pathways are activated in primary fresh DC populations remains to be determined.

Single-cell techniques have been pivotal to identify DC subsets at high resolution, establishing new molecular cell markers, and possibly inferring their ontogeny.[20,21] These studies identified a new human DC population expressing Axl (herein referred to as Axl$^+$DC). It shares markers with both plasmacytoid and conventional DC populations, but little is known about its role and functions.[20–23] We have previously established that Siglec-1, one of the few Axl$^+$DC-specific markers, efficiently mediates HIV-1 capture and infection in those cells.[24] Notably, Siglec-1 is also expressed by cervical DCs and participates in the mechanism of

[1]Institut Curie, PSL* Research University, INSERM U 932, 75005 Paris, France

[2]Laboratoire de Virologie, Hôpital Saint Louis, Assistance Publique-Hôpitaux de Paris, Paris, France

[3]INSERM U944, Université de Paris, Paris, France

[4]Vaccine Research Institute, Institut National de la Santé et de la Recherche médicale (INSERM), Assistance Publique Hôpitaux de Paris (APHP), Hôpital H. Mondor, Créteil, France

[5]Singapore Immunology Network (SIgN), A*STAR, 8A Biomedical Grove, Immunos Building, Level 4, Singapore 138648, Singapore

[6]Shanghai Institute of Immunology, Department of Immunology and Microbiology, Shanghai Jiao Tong University School of Medicine, Shanghai 200025, China

[7]Translational Immunology Institute, SingHealth Duke-NUS Academic Medical Centre, Singapore 169856, Singapore

[8]These authors contributed equally

[9]These authors contributed equally

[10]Present address: Neuroimmunology Unit, Department of Clinical Neuroscience, Karolinska Institutet, Center for Molecular Medicine L8:04, 171 76 Stockholm, Sweden

[11]Lead contact

*Correspondence: nicolas.ruffin@ki.se (N.R.), philippe.benaroch@curie.fr (P.B.)

https://doi.org/10.1016/j.isci.2023.106019

CD4$^+$T cell *trans*-infection,[25,26] further pointing to the relevance of understanding viral sensing by Axl$^+$DCs. Infected Axl$^+$DCs were efficient at transmitting newly formed HIV-1 infectious particles to activated CD4$^+$ T lymphocytes. Of note, HIV-1 assembly in Axl$^+$DCs occurs in apparently internal compartments previously observed in macrophages, whereas the assembly process in cDC2 occurs at the plasma membrane in a polarized manner similar to what is observed in infected CD4$^+$T lymphocytes. In addition, whereas Axl$^+$DC activation through Toll-like receptor (TLR) inhibits their infection by preventing viral fusion, activated Axl$^+$DCs still support HIV-1 transmission to CD4$^+$ T lymphocytes via Siglec-1,[24] in a process called *trans*-infection.[27] Axl$^+$DCs may thus participate in HIV-1 infection and spread into the host.

Among the other blood DC populations, cDC2 (CD1c$^+$ DCs) are also susceptible to HIV-1 infection, whereas cDC1 (CD141$^+$ DCs) and plasmacytoid DCs (pDCs) are resistant.[11,24,28] When exposed to HIV-1, pDCs develop a TLR7-mediated strong type I IFN response,[8,11] whereas cDC2 require Vpx to exhibit an increase in CD86 expression and IP-10 production.[11] cDC1 response to HIV-1 in the presence of Vpx is independent of viral replication and remains lower in intensity than the cDC2 response, suggesting a link between viral replication and the response observed in cDC2.[11] Similar to what has been described in MDDCs, innate sensing in cDC2 occurs via the cGAS-STING pathway with the detection of cytosolic viral cDNA.[11,29]

Given the complex role of DC populations in HIV-1 infection that can favor the initial phases of the infection but can also elicit innate and adaptative anti-viral responses,[30,31] it was of interest to evaluate the Axl$^+$DC innate response to incoming HIV-1 particles that we showed can fuse very efficiently with these cells.[24] Here, we investigated the response of *ex vivo* isolated Axl$^+$DCs on HIV-1 exposure, the sensing pathways involved, and the impact on Axl$^+$DC capacity to activate CD4$^+$ T lymphocytes. We discovered that sensing of HIV-1 is set up by Axl$^+$DCs ahead of viral replication and that two independent responses are triggered in different Axl$^+$DCs. The main response of Axl$^+$DCs exposed to HIV-1 includes activating the STAT and IRF transcription factors responsible for interferon-stimulated genes (ISG) expression. The second response is characterized by the activation of the NF-κB transcription factor that leads to the maturation of Axl$^+$DCs. Such responses were characterized computationally using complementary approaches and validated *in vitro*.

RESULTS

Axl$^+$DCs exhibit a more robust and broader innate response to HIV-1 exposure among the blood DC subsets

To better characterize the interplay between HIV-1 and primary DCs, we investigated the transcriptional response of sorted blood DCs following HIV-1(NL-AD8) exposure by bulk RNA sequencing (RNA-seq) (Figures 1A, S1A, and S1B). Levels of HIV-1 transcripts were roughly similar in Axl$^+$DC, pDC, and cDC2 subsets (Figure 1B), but cDC1 showed low levels of viral transcripts, in line with their resistance to viral fusion.[11] Both cDC1 and cDC2 poorly responded to HIV-1(NL-AD8), with none and 21 differentially expressed genes (DEGs), respectively, when compared with mock controls (Figures 1C, S1C, and Table S1). In contrast, HIV-1 exposure induced in Axl$^+$DCs and pDCs pronounced changes in gene expression (Figures 1A, 1C, S1C, and Table S1), including increased levels of inflammatory cytokines (*CCL3*, *CCL4*, and *CCL5*). Type I IFN *genes* and *CXCL10* were among the DEGs found in pDCs, consistent with a study on HIV-1-infected patients.[32] HIV-1-exposed Axl$^+$DCs expressed *CCL17* and *CCL22* genes, that encode ligands for CCR4 acting as T cell chemoattractant in inflammatory responses. HIV-1 also induced TNFα signaling and IFN responses in Axl$^+$DCs and pDCs (see GSEA on DEGs, Figure 1D).

We also evaluated the impact of Vpx on the HIV-1-induced response in the only two DC subsets that supported viral replication: Axl$^+$DCs and cDC2. The presence of Vpx induced higher viral replication, particularly in Axl$^+$DCs, and led to more extensive changes in gene expression in both cell types, amplifying the responses induced by HIV-1 (Figures 1A–1D, S1B–S1E, and Table S1). In cDC2, the addition of Vpx resulted in the expression of inflammatory genes and ISGs, demonstrating that HIV-1 sensing can occur in these cells only upon viral replication, similar to previous reports in MDDCs.[12,18]

Importantly, the addition of inhibitors of retrotranscription (azidothymidine (AZT) and nevirapine (NVP)) completely abrogated the cDC2 response to HIV-1+Vpx (Figures 1A and S1E) but did not prevent Axl$^+$DCs to activate inflammatory and IFN responses (Figures 1D and S1E). This suggested that Axl$^+$DCs can sense incoming viral particles before they start retrotranscription. HIV-1-exposed Axl$^+$DCs also upregulated genes belonging to the cytosolic sensing pathways, and the NF-κB and TNF signaling pathways (see KEGG pathway enrichment analysis on DEGs, Figure S1I, Tables S2, and S3). In addition, Axl$^+$DCs

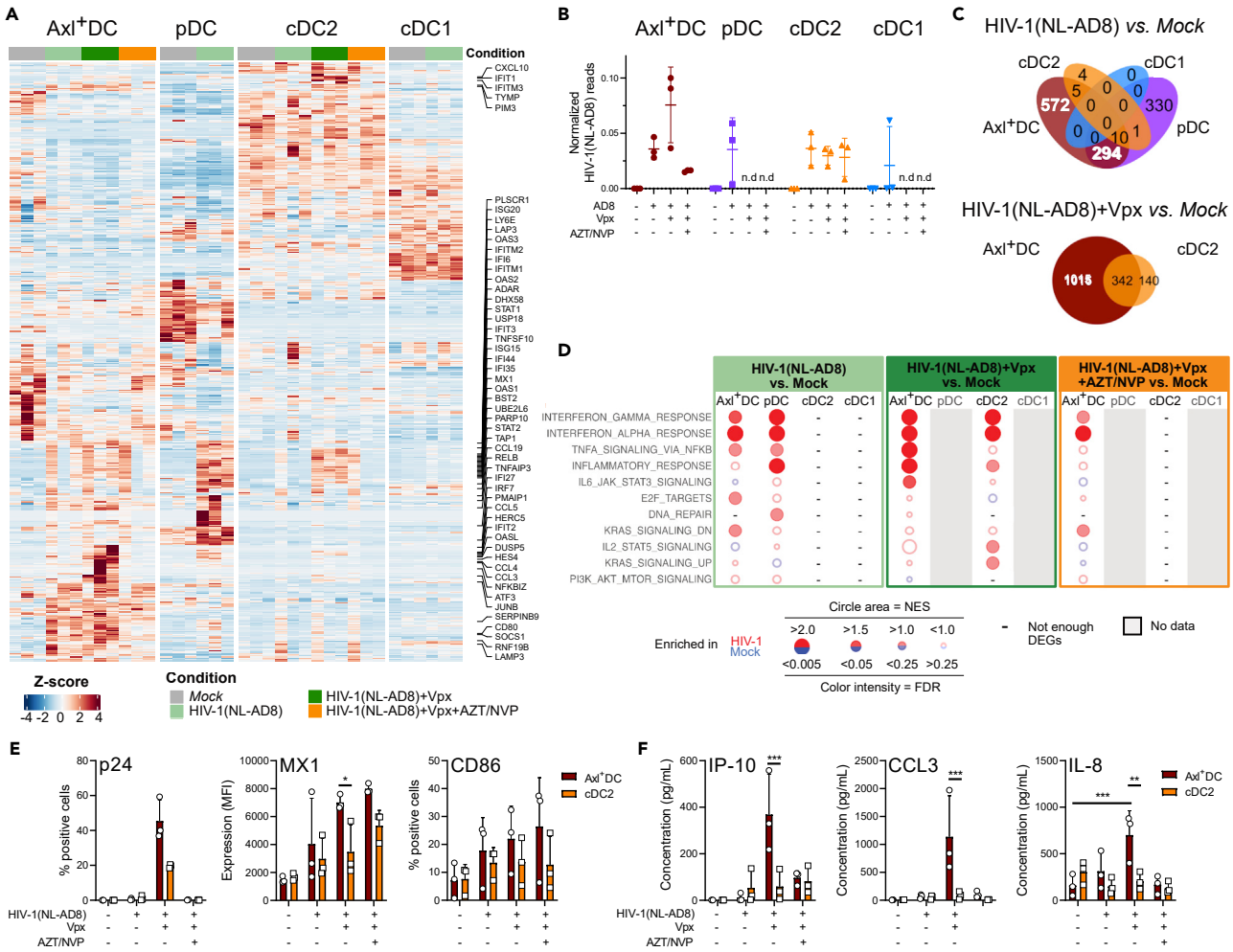

Figure 1. HIV-1 induces in blood Axl$^+$DC an innate response broader than in other blood DC subtypes

Bulk RNA-seq was performed on purified Axl$^+$DCs (Axl$^+$CD123$^+$CD33^{int}HLA-DR$^+$Lin^{neg}), pDCs (CD123$^+$Axl$^-$CD33$^-$CD45RA$^+$HLA-DR$^+$Lin^{neg}), cDC2 (CD1c$^+$CD33$^+$HLA-DR$^+$Lin^{neg}) and cDC1(CLEC9A$^+$CD1c$^-$CD33$^+$CD123$^-$HLA-DR$^+$Lin^{neg}) infected or not for 24 h with HIV-1(NL-AD8). See also Figure S1. Two additional conditions were included for Axl$^+$DCs and cDC2, which are the two subsets of HIV-1-sensitive DCs, namely HIV-1(NL-AD8)+Vpx, with or without AZT/NVP treatment.

(A) Heatmap of mean-centered and scaled Transcripts per Million (TPM) (Z score) of DEGs from each HIV-1 condition versus mock comparison in the 4 DC subtypes indicated. DEGs are defined as genes with |log2FC| > 1 and an adjusted p value <0.05 (Benjamini-Hochberg correction), n = 3 independent donors.

(B) Quantification of HIV-1 total reads among infected or non-infected DC subtypes as indicated, n= 3 independent donors. Individual donors are displayed with bars representing SD.

(C) Venn diagrams displaying the number of upregulated DEGs obtained in the four DC subtypes when comparing HIV-1(NL-AD8) (upper diagram) or HIV-1(NL-AD8)+Vpx (lower diagram) versus mock. See also Figures S1F–S1H.

(D) Bubble Map displaying top Hallmarks significantly enriched in GSEA analysis performed on ranked DEGs from each of the three HIV-1 conditions vs Mock for the 4 DC subtypes. Normalized enriched scores (NES) are represented by the area of the circles whereas log10-transformed false discovery rates (FDR) by their color intensity.

(E and F) Axl$^+$DCs and cDC2 were infected or not with HIV-1(NL-AD8) complemented or not with Vpx and treated or not with AZT/NVP for 48 h. Expression of p24, MX1 and CD86 (E) measured by flow cytometry or quantification of CXCL10/IP-10, CCL3/MIP1α and CXCL8/IL-8 (F) by CBA assay. n = 3 independent donors. Individual donors are displayed with bars representing means ± SD. Significant differences are indicated: *p < 0.05, **p < 0.01 and ***p < 0.001. See alsoFigure S1.

exhibited activation of the pathways of the cytosolic RNA sensor RIG-1 (retinoic acid-induced gene I) and Toll-like receptors (TLR) (Figures S1I and S1J).

We confirmed at the protein level the preferential activation of ISGs and inflammatory pathways in Axl$^+$DCs compared to cDC2 by measuring the expression of MX1/IP-10/CCL3 and CD86/IL-8, respectively, by flow

cytometry (Figures 1E and 1F). Compared to cDC2, these activation markers were found at higher levels in Axl$^+$DC when cultured with HIV-1(AD8) in the presence of Vpx ($p < 0.05$), except for CD86 expression, for which the significance was not reached ($p = 0.8113$).

Thus, these results indicate that Axl$^+$DCs are unique among DC subsets in the magnitude and amplitude of their response to HIV-1 exposure. This response includes activating various sensors and signaling pathways, even before HIV-1 retrotranscription.

HIV-1 exposure activates two responses in Axl$^+$DCs, distinct from the one induced by viral replication

To analyze in Axl$^+$DCs the relation between the different sensors and signaling pathways activated by HIV-1 exposure, we performed single-cell RNA-seq using a droplet-based single-cell 3′ assay (10x Genomics). We cultured Axl$^+$DCs isolated from a healthy donor with or without Vpx-complemented HIV-1(NLAD8) for 12h or 24h, in the presence or not of AZT/NVP for 24h. We obtained a total of 2983 cells from these five samples after excluding low-quality cells (see STAR Methods). Quantification of viral sequences in the 24-HIV sample (Axl$^+$DCs exposed to HIV-1 for 24h) revealed a bimodal distribution (Figure 2A), allowing for discrimination of productively infected cells (i.e., cells with a viral UMI fraction >1.58%), containing both viral mRNA and genomic RNA, from cells that only contained viral genomic RNA from up taken virions. Notably, the amount of productively infected cells measured by scRNA-seq data was consistent with the levels of *gag*-encoded protein p24$^+$ Axl$^+$DCs measured by flow cytometry at 48h post-infection (p.i.) (Figure 2B). Spliced viral sequences (Figure S2A) were exclusively detected in cells with a high proportion of viral transcripts further supporting that viral replication had taken place in these cells. The relative contribution of each HIV-1 gene to the total viral transcripts across the productively infected cells was independent of the amount of viral mRNA in the cell (Figure S2A). Our results indicate that cells containing incoming viral particles can be distinguished from cells experiencing active viral replication by scRNA-seq.

Clustering the five pooled Axl$^+$DC samples in a reduced transcriptomic space (see STAR Methods) identified four clusters of cells (Figures 2C, S2B, and Table S4). A substantial fraction of Axl$^+$DCs exposed to HIV-1 for 12 h was transcriptionally similar to the population of non-exposed cells (cluster 1, Figures 2C and S2B). In contrast, all Axl$^+$DCs responded to HIV-1 after 24 h of exposure and were distributed in three different clusters independently of the presence of retrotranscription inhibitors. Most productively infected cells were found in cluster 4 (Figures 2D and S2C). Thus, Axl$^+$DCs established three distinct transcriptional programs in response to HIV-1 exposure, including an early response starting at 12 h (cluster 2). We ruled out that this early response was due to a higher viral uptake by Axl$^+$DCs because there was no apparent difference in the viral transcript fraction between clusters 1 and 2 from Axl$^+$DCs cultured with HIV-1 for 12 h (Figure S2D). AZT/NVP did not modify the transcriptional response of HIV-1-exposed Axl$^+$DCs, which remained grouped in clusters 2 and 3 (Figures 2C and S2B), suggesting that Axl$^+$DCs can respond to incoming viral particles independently of retrotranscription. Although most productively infected Axl$^+$DCs were found in cluster 4, the remaining ones were mostly found in cluster 3, with fewer viral transcripts (Figures S2C and S2E), possibly reflecting a difference in the dynamics of the HIV-1 replication cycle.

Thus, the response of Axl$^+$DCs to HIV-1 appears heterogeneous. Viral exposure activates two distinct transcriptional programs in a retrotranscription-independent manner, whereas productive HIV-1 replication triggers another specific program.

In cluster 2, we identified markers of DC maturation (*CCR7*, *CD83*, *CD70*) and activation (*CCL17*, *CCL22*) (Figures 2E, S2F, and Table S4). The transcription factors *NFKB1*, *NFKB2*, *RELA*, and *REL* were up regulated in cluster 2, consistently with the enrichment of genes involved in T cell help (Figures 2F, S2F, and S3A). Functional annotation of cluster 2-specific DEGs confirmed an enrichment in genes involved in the TNF/NF-κB pathway and T cell activation process (Figure S2G). In contrast, Axl$^+$DC cluster 3 exhibited an increased expression of 46 genes classified as ISGs,[33] including *IFI6*, *IFI44L*, *MX1*, *BST2*, and the transcription factor *STAT1* (Figures 2E, S2F, S2H, S3B, and S3C).

The response of Axl$^+$DC cluster 4 was broader and more robust, encompassing the same ISGs as in cluster 3 but also 44 additional ones (Figures 2G, S2I, S3B, and S3C). In addition, Axl$^+$DC cluster 4 highly expressed inflammatory cytokines (*CCL4*, *IL1B*, and *TNF*) and genes involved in DC maturation (e.g., *CCR7* and *CD86*). These cells also expressed the transcription factors *STAT1/2* and *IRF7*, as well as *NFKB1* (Figures 2E and

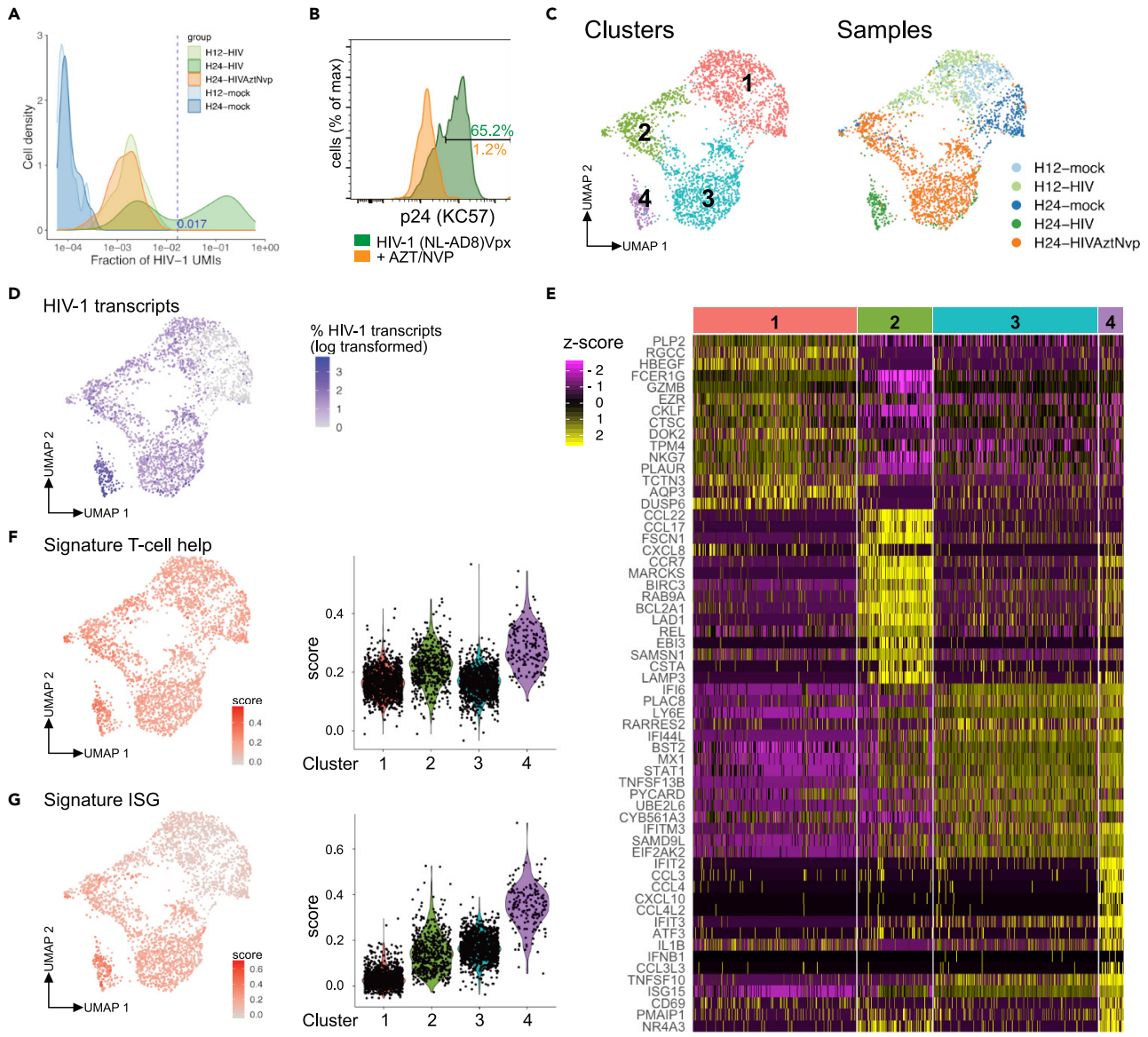

Figure 2. HIV-1 exposure of Axl^{+}DCs induced two transcriptional responses

Purified Axl^{+}DCs (AXL^{+}CD123^{+}CD33^{int}HLA-DR^{+}Lin^{neg}) were cultured for 12 or 24 h in the presence or not of HIV-1(NL-AD8), HIV-1(NL-AD8)+Vpx with or without AZT/NVP treatment before being processed for single-cell RNA sequencing.

(A) Distribution of the HIV-1 viral UMI (unique molecular identifier) fraction computed over the total UMI counts across cells. The dashed blue line separates productively and non-productively infected cells (see STAR Methods).

(B) Quantification of p24 (by FACS) in Axl^{+}DCs infected with HIV-1(NLAD8)+Vpx (green) or HIV-1(NL-AD8)+Vpx and AZT/NVP (orange) for 48 h. Same donor as in scRNA-seq.

(C) Uniform Mani-fold Approximation and Projection (UMAP) of the five pooled scRNA-seq samples, colored either by cluster (left panel) or by sample (right panel). (See STAR Methods for cluster determination).

(D) UMAP colored by viral HIV-1 UMI fraction, scaled and log10-transformed.

(E) Heatmap of log-transformed normalized expression levels (*Z* score) of the top 10 significant DEGs in each cluster (see top annotation) with respect to their complementary (log2FC > 0, adj. p value <0.05, detected in >50% of the cells in the cluster). DEGs found in more than one comparison are reported only once.

(F and G) UMAP plots (left) and violin plots (right) of (F) T cell Help Signature score and (G) ISG signature score in individual cells and clusters, respectively. See also Figures S2–S4, and Table S4.

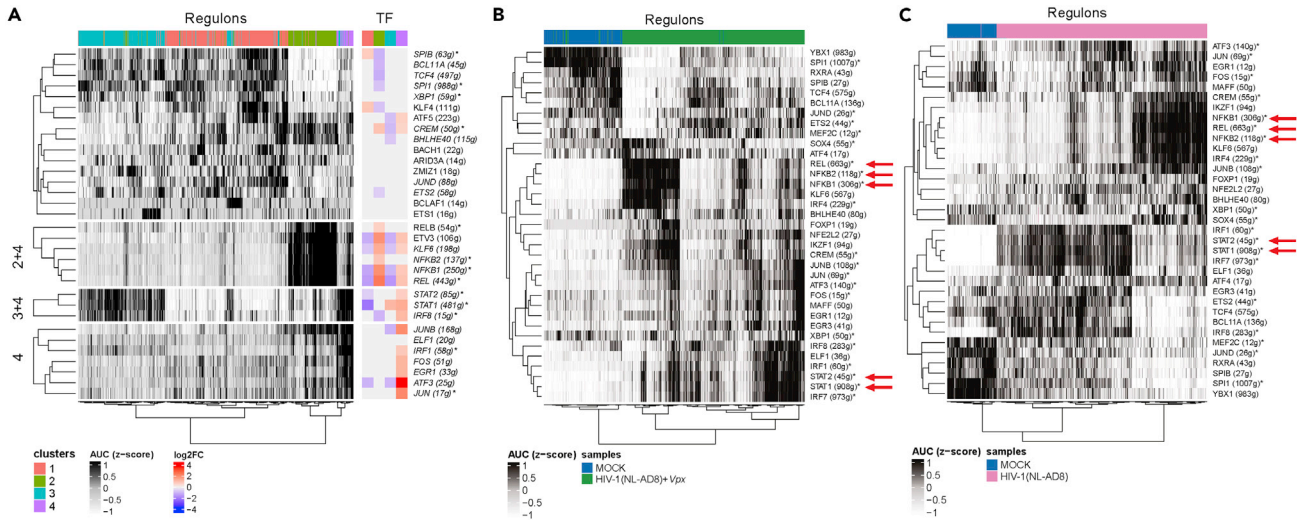

Figure 3. Identification of key transcription factors involved in the Axl$^+$DC response to HIV-1 exposure

(A) Gene network inference analysis. Left: heatmap of AUC (*Z* score) of regulon-cell pairs (a regulon is a set of genes regulated by the same transcription factor, TF). Cells are annotated according to the cluster they belong, and regulons are labeled by the corresponding TF (the number of genes is reported in parentheses). Rows and columns are clustered using Ward's minimum variance method computed on Euclidean distances. Right: heatmap of significant (adjusted p value <0.05) log2FC values for the TFs between each cluster and its complementary. Regulons supported by high-confidence TF binding motif annotations are marked with an asterisk (see STAR Methods) and those detected in both replicates are shown in italic.

(B) Heatmap of AUC (*Z* score) of regulon-cell pairs for gene network inference analysis of the scRNA-seq dataset replicate 2 as in A, between mock (blue) and HIV-1(NL-AD8)+Vpx (green) samples.

(C) Heatmap of AUC (*Z* score) of regulon-cell pairs for gene network inference analysis of the scRNA-seq dataset replicate 2 as in B, between mock (blue) and HIV-1(NL-AD8) (pink) samples.

See also Figure S5.

S2F). We confirmed by flow cytometry the higher expression of MX1, CD86, and CCR7 on infected Axl$^+$DC as compared to bystander non-infected cells, although the difference observed lacked statistical significance (Figure S4).

These results reveal that HIV-1 particles induce in Axl$^+$DCs two main responses characterized by ISGs and genes involved in T cell help, respectively. Notably, both responses took place in different cells and were retrotranscription-independent. However, both responses were likewise activated in Axl$^+$DCs that underwent active viral replication.

Identification of key transcription factors involved in the Axl$^+$DC responses to HIV-1 exposure

To determine the critical transcription factors involved in the heterogeneous Axl$^+$DC response to HIV-1, we performed gene network inference using SCENIC.[34] The clustering inferred from transcription factor activity was very similar to the one directly obtained from gene expression (Figure 3A), allowing us to link the markers detected above with their putative regulators. Cluster 2 displayed high activity of canonical (*NFBK1* and *REL* regulons) and non-canonical (*NFKB2* and *RELB* regulons) NF-κB pathways, as well as pathways involving *ETV3* and *KLF6* (Figures 3A and S5A). Notably, the transcription factors responsible for the expression of these regulons were upregulated in cluster 2 and, except for *NFKB2* and *RELB*, also in cluster 4 (Figure 3A). Thus, in cluster 2, HIV-1 entry induced the activation of NF-κB pathways in a retrotranscription-independent manner (Figure 2C). Of interest, the regulons activated in cluster 3 were also found in cluster 4 and covered genes regulated by STAT1, STAT2, and IRF8 with the STAT1 regulon encompassing the highest number of genes (481 genes) (Figures 3A and S5A). In addition, Axl$^+$DC cluster 4 response also encompassed FOS/JUN, IRF1, and ATF3 regulons.

Integrating the clustering and the regulon analyses, we identified for each of the two transcriptional programs observed in Axl$^+$DCs exposed to HIV-1, the transcription factors potentially involved. The ISG response appeared driven by STAT1/2 and IRF, whereas the T cell help signature by NF-κB1/2.

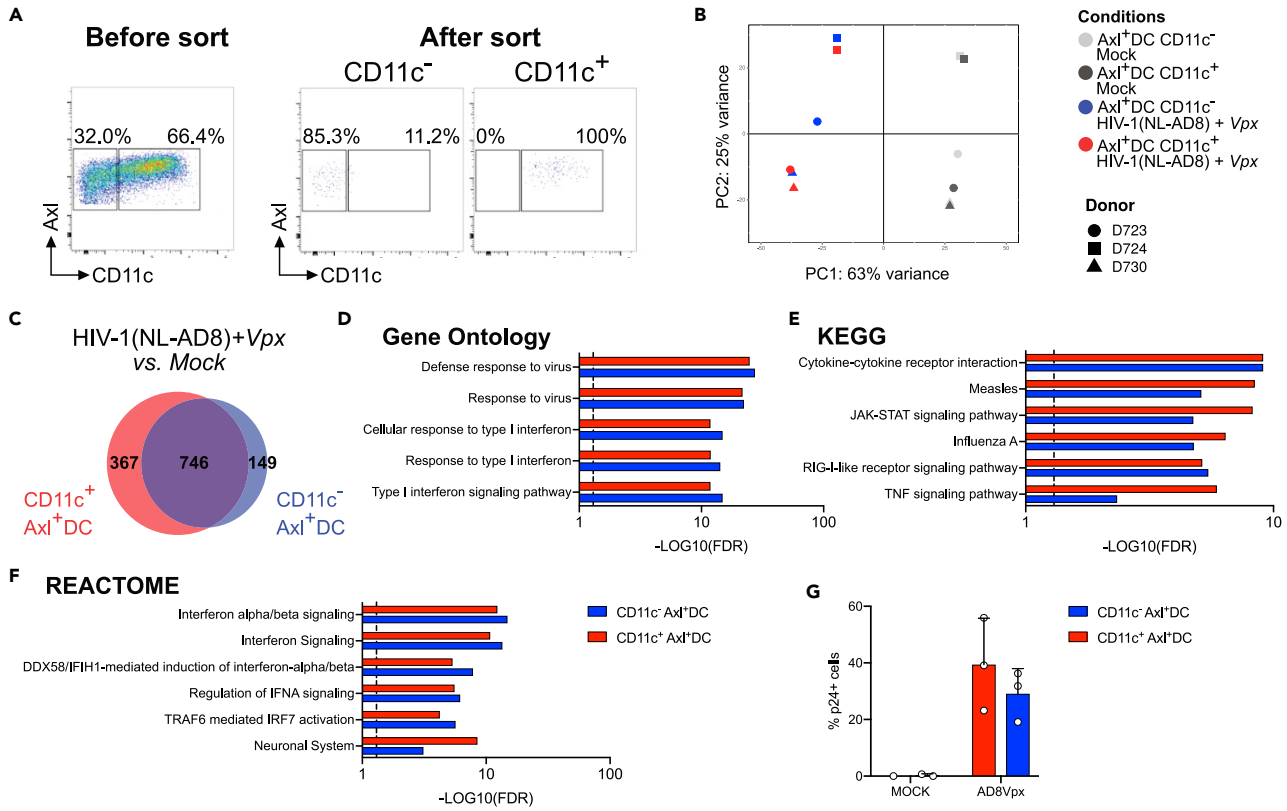

Figure 4. Axl$^+$DC responses to HIV-1 are independent of CD11c expression

Bulk RNA-seq was performed on sorted CD11c$^+$Axl$^+$DC and CD11c$^-$Axl$^+$DC exposed to HIV-1(NL-AD8)+Vpx or not for 24 h.

(A) Representative dot plot of CD11c and Axl expression in Axl$^+$DCs before and after sorting cells by FACS.

(B) PCA visualization of bulk RNA-seq samples. n = 3 independent donors. Samples projection is computed based on the top 500 varying genes. The shape of each point corresponds to the cohort donors, and the points are colored by Axl$^+$DC culture conditions.

(C) Venn diagram displaying DEGs obtained in CD11c$^+$ Axl$^+$DCs (red) or CD11c$^-$Axl$^+$DCs (blue) when comparing HIV-1(NL-AD8)+Vpx versus mock.

(D) Top 5 pathways from GO (Biological processes), (E) KEGG and (F) REACTOME databases enriched in DEGs obtained in CD11c$^+$Axl$^+$DCs (red) or CD11c$^-$Axl$^+$DCs (blue) when comparing HIV-1(NL-AD8)+Vpx versus mock. Bar plots represent log10-transformed FDR. The dashed line represents an FDR cut-off of 0.05.

(G) Expression of p24 measured by FACS in CD11c$^+$ (red) and CD11c$^-$ (blue) Axl$^+$DCs mock or exposed to HIV-1 for 48 h. Individual donors are displayed with bars representing means ± SD.

To evaluate the impact of Vpx in Axl$^+$DC responses, we performed a second scRNA-seq experiment on Axl$^+$DCs exposed to HIV-1(NL-AD8) in the absence or presence of Vpx for 24 h. We projected the cells to the clusters obtained for the first experiment using scMAP.[35] Most of the cells in this second experiment could be assigned to the transcriptomes identified in the first experiment. HIV-1(Vpx) induced in Axl$^+$DCs the three different transcriptional programs that matched the ones observed in the first experiment (Figures 2 and S5B). Notably, similar results were obtained for cells exposed to HIV-1 in the absence of Vpx (Figure S5C). Gene network inference also confirmed the induction of the two different transcriptional programs previously observed, involving the activation of the NF-κB pathways or STAT1/2 and IRF, leading to ISG expression (Figures 3B and 3C).

Axl$^+$DC response to HIV-1 is independent of CD11c expression

Axl$^+$DCs have been proposed to represent a mix of cells sharing characteristics closer to cDC2 or pDCs based on the presence or absence of CD11c expression.[21,23] To determine whether the dual response we observed in Axl$^+$DCs exposed to HIV-1 comes from this heterogeneity, Axl$^+$DCs were sorted into CD11c$^+$ and CD11c$^-$ cells, cultured for 24 h with HIV-1 and analyzed by RNA-seq (Figure 4A). Principal component analysis (PCA) based on the top 500 variable genes revealed indistinguishable responses to HIV-1 exposure in both cell populations (Figure 4B). The vast majority of DEGs specific for cells exposed

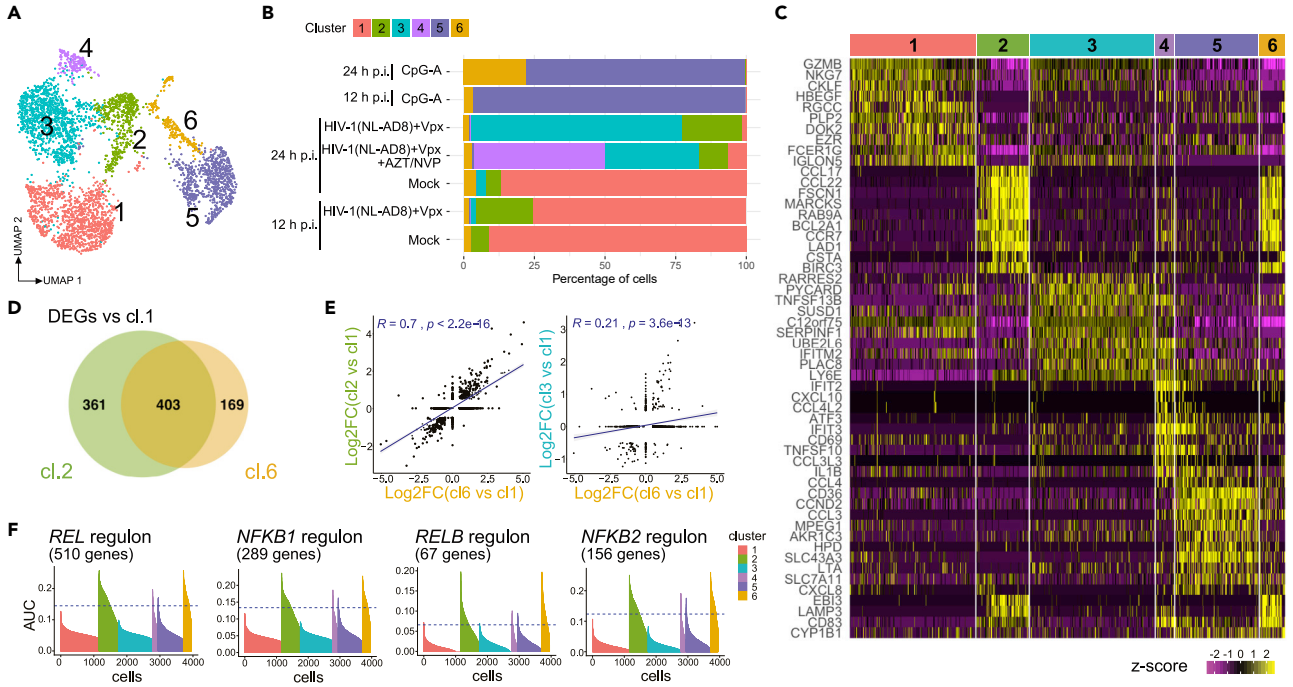

Figure 5. The NF-kB-dependent response to HIV-1 is largely phenocopied by TLR activation in Axl$^+$ DCs

Axl$^+$DCs treated with CpG-A for 12 h or 24 h were processed in parallel in the experiment depicted in Figure 2 for scRNA-seq analysis. The whole scRNA-seq dataset considered here was therefore composed of 7 samples.

(A) Dimensionality reduction by UMAP of the scRNA-seq dataset (7 samples). UMAP representation (UMAP1 and UMAP2 components) is colored by clusters.

(B) Cluster distribution within each sample.

(C) Heatmap of log-transformed normalized expression levels (*Z* score) of the top 10 significant DEGs in each cluster (see top annotation) with respect to their complementary (log2FC > 0, adj. p value <0.05, detected in >50% of the cells in the cluster). DEGs found in more than one comparison are reported only once.

(D) Venn diagram displaying DEGs obtained in cluster 2 (green) or cluster 6 (yellow) when comparing with cluster 1.

(E) Dot plot of DEGs log2FC obtained comparing clusters 2 and 6 versus cluster 1 (left panel) or comparing clusters 3 and 6 versus cluster 1 (right panel). The blue lines represent linear regressions. Pearson's correlation coefficients and p values are indicated.

(F) Waterfall plots of AUC values in each cell obtained from network inference analysis for the indicated regulon. Colors represent clusters from clustering analysis (7 samples, see Figures 5A and 5B) and the dashed blue lines define the AUC cut-off identifying the cells where the regulon is active (see STAR Methods).

to HIV-1 vs mock control were shared among the two cell populations (n = 746 DEGs out of 1113, and 895 for CD11c$^+$ and CD11c$^-$ cells, respectively, Figure 4C). Further analyses of DEGs by Gene Ontology, REACTOME or KEGG databases showed that both CD11c$^+$ and CD11c$^-$ Axl$^+$DCs responded to HIV-1 by inducing the expression of genes involved in type-I IFN signaling, TLR, and TNF signaling (Figures 4D, 4E and 4F), consistent with our results (Figures 1 and 2). Both CD11c$^+$ and CD11c$^-$ Axl$^+$DCs were susceptible to HIV-1 infection, as measured by HIV-1 p24 protein expression (Figure 4G). Thus, the dual response observed following Axl$^+$DC culture with HIV-1 is unlikely to arise from differences in CD11c expression.

HIV-1 sensing by Axl$^+$DCs activates the NF-κB pathway, possibly via TLR triggering

TLR signaling was identified as one of the major pathways involved in the response of Axl$^+$DCs to HIV-1 (Figures S1I and S1J). Hence, we generated two additional samples; Axl$^+$DCs stimulated with a TLR9-ligand (CpG-A) for 12 and 24 h. We merged them with the five samples previously processed and found two new clusters in addition to the four previously obtained (Figures 2C and 5A). Most cells from the two CpG-A stimulated samples clustered together (in cluster 5), except for a minor part of Axl$^+$DCs stimulated by CpG-A for 24h, which showed a distinct transcriptome (cluster 6; see Figures 5B and 5C). Notably, markers of clusters 6 and 2 highly overlapped (Figures 5C and 5D), and their relative expression was positively correlated (Figure 5E). The cells stimulated by CpG-A for 24h showed a high expression of the maturation

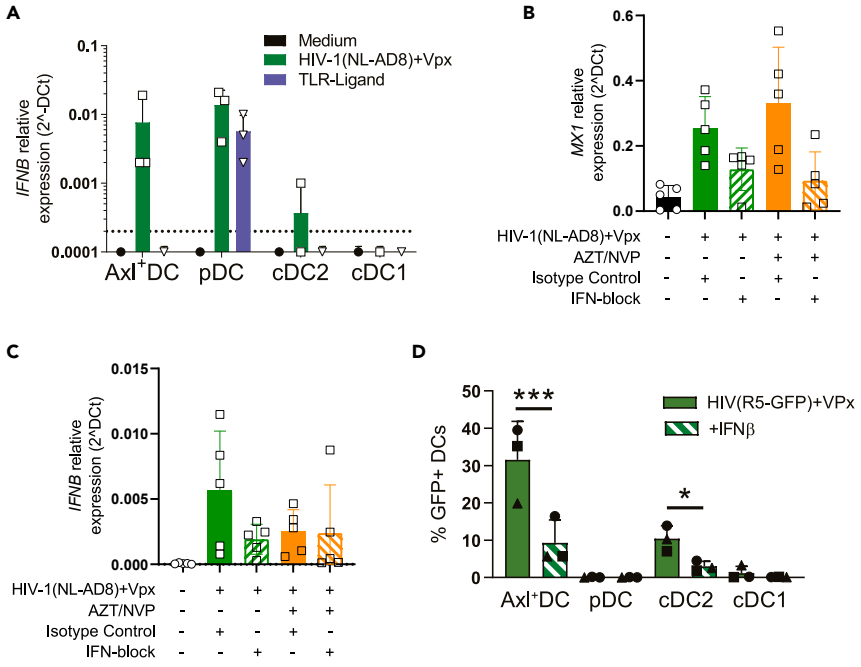

Figure 6. HIV-1 induces IFNβ expression in Axl$^+$DCs

(A) *IFNB1* relative expression measured by RT-qPCR in the 4 DC subsets infected or not with HIV-1(NL-AD8)+Vpx or treated with TLR ligands (CpG-A for Axl$^+$DCs and pDCs, and R848 for cDC1 and cDC2), n = 3 independent donors.
(B) *MX1* and (C) *IFNB* relative expression measured by RT-qPCR in Axl$^+$DCs exposed or not with HIV-1(NL-AD8)+Vpx, and treated or not with AZT/NVP or with a cocktail of type I IFN blocking antibodies, n= 5 independent donors.
(D) Quantification of GFP expression in sorted DC subsets, treated with medium or IFNβ, before infection with HIV-1 R5GFP for 48h. n = 3 independent donors, *p<0.05 and ****p<0.0001. Individual donors are displayed with bars representing means ± SD.

markers *CCR7*, *CD83*, *CD40*, and the cytokines *CCL17* and *CCL22*, all involved in T cell priming. Then, by computing regulon activity in CpG-A-stimulated cells, we found that NF-κB-regulated genes were specifically induced in both clusters 2 and 6, and the extent of the response was highly similar between the two clusters (Figure 5F).

Thus, the transcriptional response observed in Axl$^+$DCs following 12 and 24 h culture with HIV-1 suggests that HIV-1 activates TLR signaling in this cell subset.

HIV-1 induces IFNβ expression in Axl$^+$DCs

Consistent with our previous results,[20] CpG-A stimulation of pDCs and Axl$^+$DCs, raised high levels of *IFNB* transcripts in pDCs but no detectable levels in Axl$^+$DCs, confirming the absence of contamination by pDCs in our Axl$^+$DC preparation and thus validating our purification strategy (Figure 6A). In contrast, upon HIV-1 exposure, Axl$^+$DCs expressed *IFNB* mRNA as seen by qPCR (Figure 6A) and scRNA-seq (Table S4). Of note, the levels of *IFNB* mRNA induced by HIV-1 were similar between Axl$^+$DCs and pDCs, in contrast to cDCs for which *IFNB* expression was absent (Figure 6A). We also confirmed that type I IFN plays a crucial role in the induction of ISGs following HIV-1 sensing. The use of a blocking antibody cocktail against IFNα, IFNβ and IFNαβ receptor led to a decrease in *MX1* expression induced by HIV-1, independently of viral replication (Figure 6B). We noted variability among donors regarding the efficiencies of IFN-blocking which may reflect that traces of type I IFN are sufficient to induce an ISG response. The induction of *IFNB* gene expression was also prevented by the IFN-blocking reagents in Axl$^+$DCs with active HIV-1 replication (Figure 6C). *IFNB* and ISG expression being the highest in cells with active viral replication, we evaluated the anti-viral effect of IFNβ on purified Axl$^+$DCs before HIV-1 exposure. HIV-1 replication was prevented in Axl$^+$DCs and cDC2 when treated with IFNβ (Figure 6D), confirming, in these cells, that type I IFN confers protection to HIV-1 before infection. However, once cells are infected, ISG induction no longer protects the infected cells from HIV-1 replication.

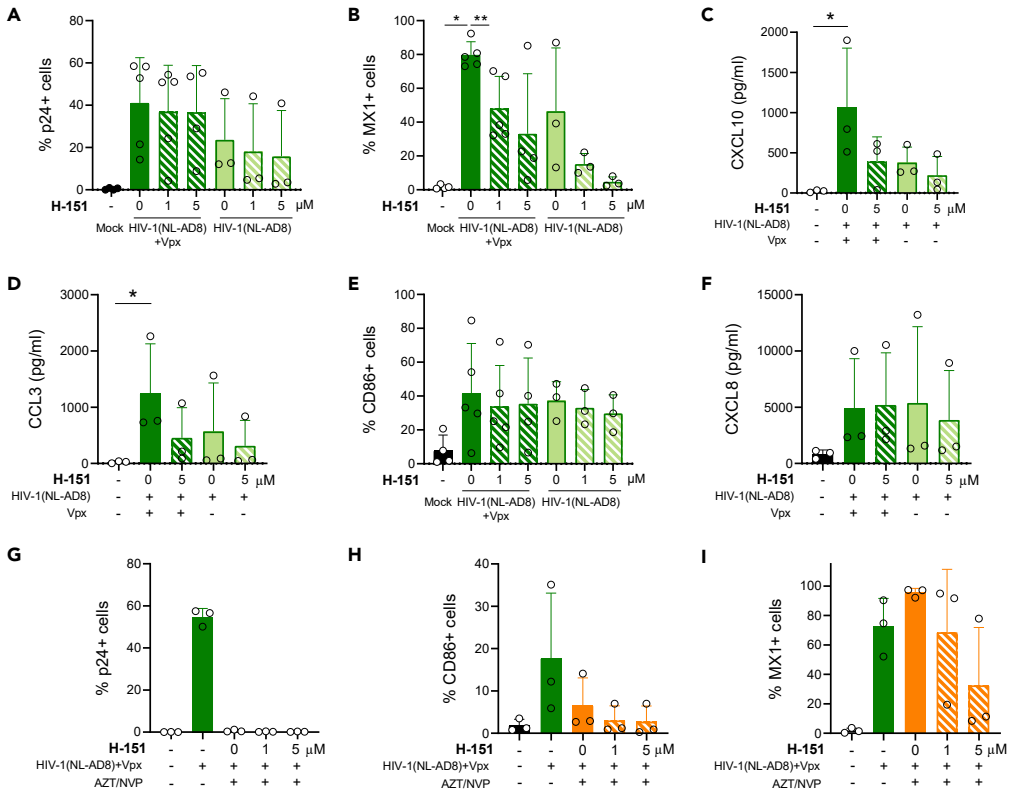

Figure 7. STING activation plays a role in the induction of ISG in HIV-1-exposed Axl$^+$DCs

Axl$^+$DCs were treated with the STING antagonist H-151 at different doses and for 30 min before exposure to HIV-1(NL-AD8)+Vpx. After 48 h, cell marker expression and CBA were performed by flow cytometry. (A to F) Percentages of expression of the indicated proteins or amounts of the indicated proteins secreted among the various cell populations are displayed. n = 3 to 5 for HIV-1(NLAD8)+Vpx samples and n= 3 for HIV-1(NLAD8) samples.

(G–I) Axl$^+$DCs were treated with different doses of STING inhibitor H-151 for 30 min before exposure to HIV-1(NL-AD8)+Vpx in the presence or absence of AZT/NVP, for 48 h. Expression of p24 (G), CD86 (H) and MX1 (I) was measured by FACS, n = 3 independent donors.

Individual donors are displayed with bars representing mean ± SD, significant differences are indicated: *p< 0.05, **p< 0.01.

STING activation is involved for the induction of ISG in HIV-1-exposed Axl$^+$DCs

STING activation being central in the ISG response induced by HIV-1 in MDDC,[36] we tested its involvement in HIV-1 sensing by Axl$^+$DCs. In Axl$^+$DCs exposed to HIV-1 in the presence or not of Vpx, the inhibition of STING did not impact HIV-1 replication measured by p24 expression (Figure 7A) but led to a significant decrease of MX1 expression as well as lower CXCL10 (IP-10) and CCL3 secreted levels (Figures 7B, 7C, and 7D). Levels of CD86 expression and CCL8 production remained unaffected by STING inhibition (Figures 7E and 7F). The addition of AZT/NVP completely abrogated HIV-1 replication in Axl$^+$DCs, decreased CD86 expression, but did not impact the high levels of MX1 expression (Figures 7G, 7H, and 7I). The addition of retrotranscription and STING inhibitors to HIV-1-exposed Axl$^+$DCs reduced MX1 expression, although not significantly (Figure 7I). These results confirmed that Axl$^+$DCs can sense incoming viral particles independently of the retrotranscription. They also indicate that following HIV-1 sensing, STING is critical in inducing ISG expression.

Priming of CD4$^+$ T cells by HIV-1-exposed Axl$^+$DCs

To evaluate at the functional level the impact of HIV-1 on Axl$^+$DCs, we tested their capacity to prime T cells in co-culture experiments (Figure 8A). To bypass the problem of MHC restriction (and nominal antigen) with human cells, we used the superantigen TSST-1 (toxic shock syndrome toxin) that binds to a constant region of the MHC class II β chain present on DCs and can stimulate roughly 15% of human blood T cells via their TCR providing they express Vβ2 and that DCs provide an efficient co-stimulatory signal.[37] Comparing blood DC subsets on the addition of TSST-1, Axl$^+$DCs were able to stimulate interleukin (IL)-2 production

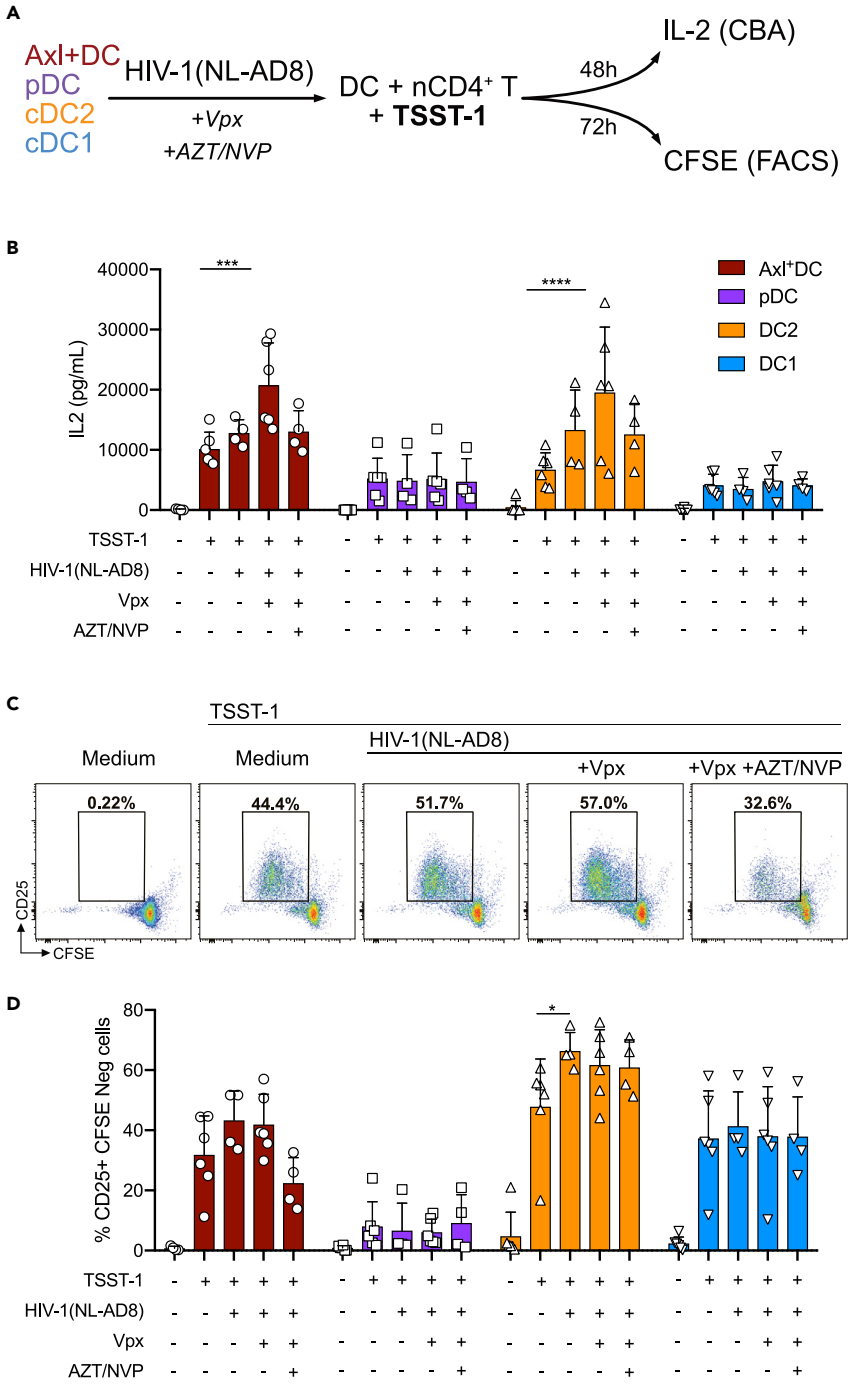

Figure 8. Axl$^+$DCs and cDC2 exposed to HIV-1 can prime naive CD4$^+$ T cells

The 4 blood DC subsets were sorted and exposed to HIV-1(NL-AD8) complemented or not with Vpx and treated or not with AZT/NVP; or were stimulated with TLR-L (CpG-A for Axl$^+$DCs and pDCs, and R848 for cDC1 and cDC2). Cells were cultured overnight, the supernatant was removed, and CFSE-stained naive CD4$^+$ T cells were added in a 1:10 ratio (1 DC for 10 T cells) in the presence of SuperAntigen TSST-1 and cultured for 48 h or 72 h for assessment of T cell proliferation.

(A) Outline of the experiment.

(B) IL-2 quantification by CBA in the supernatant of the various co-cultures at 48 h as indicated. n= 4 to 6 independent experiments.

(C) Representative dot plots of CFSE and CD25 expression in gated CD3$^+$T cells following a 72 h co-culture with Axl$^+$DCs treated as indicated.

Figure 8. *Continued*

(D) Quantification of proliferating $CD4^+$ T cells after 72 h of co-culture with uninfected or HIV-1-infected DC populations as in (C). Proliferating $CD4^+$ T cells were gated as $CD3^+CFSE^{lo/-}CD25^+$. n= 4 to 6 independent experiments. Individual donors are displayed with bars representing mean ± SD. Significant differences are indicated: *p < 0.05, **p < 0.01 ***, p <0.001 ****, and p < 0.0001.

by $CD4^+$ T cells (Figure 8B) and their proliferation, although at slightly lower levels than cDC2 (Figures 8C and 8D). Exposure of Axl^+DCs and cDC2 to HIV-1(Vpx) enhanced the IL-2 secretion by T cells (Figure 8B) and their proliferation (Figures 8C and 8D). Of note, both pDCs and cDC1 produced small amounts of IL-2 in response to TSST-1 under all conditions (Figure 8B). Still, only cDC1 stimulated $CD4^+$T cell proliferation independently of HIV-1 exposure, suggesting that pDCs cannot provide appropriate signals to stimulate T cell proliferation following HIV-1 exposure (Figure 8D). These results are consistent with the DC maturation program induced by HIV-1 observed at the mRNA and protein levels in Axl^+DC (Figure 1) and suggest a role for HIV-1 replication in the DC-priming of $CD4^+$ T cells.

Analysis of the transcriptional programs of Axl^+DCs from HIV-1-infected patients

To further evaluate whether HIV-1 also impacts Axl^+DC transcriptional program *in vivo*, we assessed DC subsets from different groups of HIV-1-infected patients (Table S5). We first assessed Axl^+DC proportion in the blood during HIV-1 infection in a cohort of patients either during primo-infection (less than three months), chronic infection or viremia suppressed with antiretroviral therapy (ART) compared to HIV-1 negative controls (Figures 9A and S6). The frequency of Axl^+DCs among blood DC subsets remained very similar in the different groups of donors/patients. Although we observed a tendency for pDC levels to slightly decrease during HIV-1 primo-infection, the differences were not statistically significant. cDC2 levels also remained homogeneous, whereas cDC1 levels were significantly increased in ART-treated HIV-1-infected patients compared to untreated patient groups either in the primo or chronic phase of the infection (Figure 9A).

We then performed scRNA-seq on sorted DC populations from an HIV-1-infected patient in primo-infection and merged with Axl^+DCs and cDC2 isolated from a healthy control (Figure 9B). In contrast to *in vitro* infected DCs and despite detectable viral load ($5.19*10^5$ copies/mL), we could not detect HIV-1 transcripts in any cell population. Importantly, we found an ISG signature in all DCs from the HIV-1-infected patient in primo-infection, with the highest levels found in cDC2 (Figure 9C). However, the T cell help signature was low or absent in the 4 DC subsets from the patient (Figure 9D). The functional analysis of the DEG between DCs from the HIV-1-infected patient and control confirmed the engagement of type I IFN signaling in Axl^+DCs and cDC2 (Figure 9E), whereas the NF-kB activity was present only in cDC2. These results and the absence of detected HIV-1 transcript in circulating primary DCs favor the hypothesis of an indirect impact of inflammation and type I IFN on DCs, without excluding the possibility of DC migration to lymphoid tissues following their encounter with HIV-1.

DISCUSSION

Here, we set out to comprehensively study the response to HIV-1 of the recently identified Axl^+DC population. We first show by RNA-seq analysis that primary Axl^+DCs exhibit a broader and stronger response on HIV-1 exposure compared to cDC2, which are also susceptible to the infection, and to pDCs and cDC1, which are not. Notably, Axl^+DC response was initiated independently from HIV-1 retrotranscription but amplified and diversified following active viral replication, pointing to the unique sensing capacities of Axl^+DCs. Then, scRNA-seq revealed that HIV-1 induced diverse transcriptional programs in Axl^+DCs confirmed by functional assays. The observed responses probably originated from different mechanisms of viral sensing and depended on the amounts of viral transcripts in each cell.

The HIV-1-induced inflammatory response observed in Axl^+DCs from cluster 2 was highly similar to the one induced by TLR stimulation, suggesting that HIV-1 sensing in the endosomal pathway could be involved. Of interest, HIV-1 replication did not occur in Axl^+DCs displaying the inflammatory response with activated canonical and non-canonical NF-κB pathways. We have previously shown that TLR stimulation switched Axl^+DC to an HIV-1-resistant state associated with potent inhibition of viral fusion,[24] but further work is needed to dissect the regulation of HIV-1 fusion following its sensing by Axl^+DCs.

In contrast, the HIV-1-exposed Axl^+DCs lacking the inflammatory program expressed instead genes dependent on STAT1, STAT2, and IRF8 transcription factors, leading to ISG responses dependent on

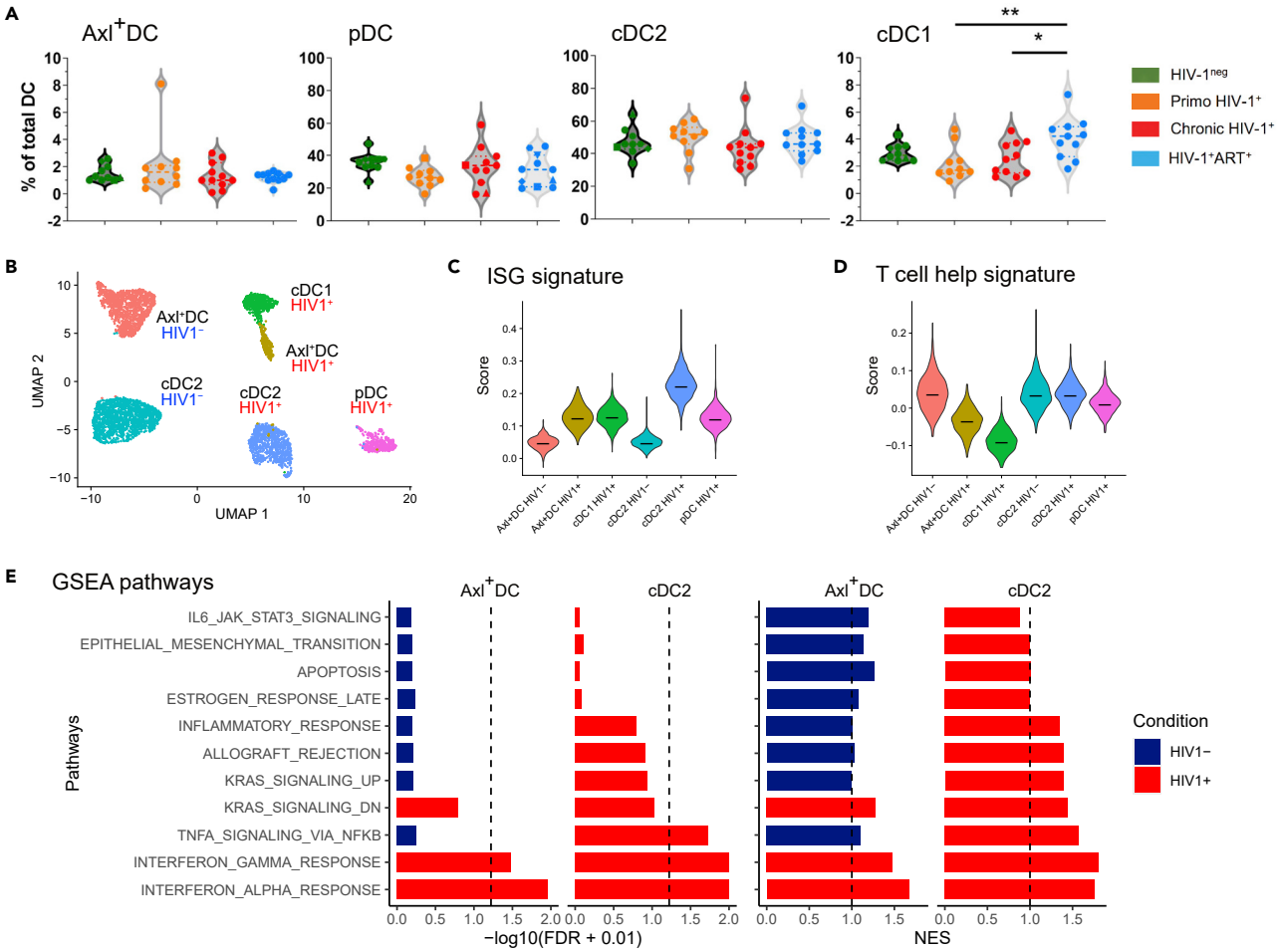

Figure 9. Axl$^+$DCs exhibit IFN and inflammatory responses in an HIV-1-infected patient

(A) Proportion of blood Axl$^+$DCs, pDCs, cDC2 and cDC1 in healthy donors or HIV-1-infected patients during primo-infection (Primo HIV-1$^+$, n = 10), chronic infection (Chronic HIV-1$^+$, n = 11) or after antiretroviral therapy initiation (HIV-1$^+$ART$^+$, n = 11), represented by violin plot with medians. Significant differences are indicated by stars, *p < 0.05 and **p < 0.01. See Figure S6 for the gating strategy used and Table S5 for cohort characteristics.

(B) UMAP of the pooled scRNA-seq samples from an HIV-1 infected individual and control cells, colored by cluster (See STAR Methods for cluster determination).

(C) Violin plots of ISG signature and (D) T cell help signature scores in individual clusters.

(E) Hallmarks significantly enriched in GSEA analysis performed on ranked DEGs obtained comparing sorted cDC2 and Axl$^+$DCs from an HIV-1-infected patient versus DCs from a healthy donor. Bar plots represent normalized enriched score (NES) and log10-transformed false discovery rate (FDR). Enrichment is considered significant when FDR <0.25 (vertical dashed line).

See also Figure S6 and Table S5.

STING activation. The ISG responses were STING-dependent and qualitatively similar, although of higher intensity, in Axl$^+$DCs with active HIV-1 replication or when retrotranscription was blocked. This result suggests that viral RNA, proviral cDNA, or transcribed viral mRNA may constitute PAMPs, eventually stimulating the STING pathway. Such responses have been previously described in MDDCs,[38] but only following HIV-1 replication. Our study reveals that Axl$^+$DCs can respond to HIV-1 in the absence of viral replication.

Of interest, NF-κB and STING pathways are interconnected because STING activation can induce the canonical NF-κB pathway via activation of the TBK1 kinase.[39] Therefore, the expression of *NFKB1* and *REL* we observed in Axl$^+$DCs with active viral replication could represent a consequence of STING activation. However, activation of the non-canonical NF-κB pathway has been reported to inhibit STING activation,[40] in line with the near complete absence of ISG response we observed in cells exhibiting an NF-κB-dependent inflammatory response. In pDCs, viral exposure engaged the cells in a progressive diversification leading to 3 populations with specific responses.[41] In contrast, our results show the appearance of diverse responses of

Axl + DCs after viral exposure as a consequence of different sensing mechanisms. Further work is required to evaluate the importance of the NF-κB/STING signaling crosstalk in primary DCs.

Using the STING inhibitor H-151, we demonstrate that STING is activated following HIV-1 sensing in Axl$^+$DCs, even in the presence of retrotranscription inhibitors. Thus, cytosolic sensing of HIV-1 RNA following viral entry may take place in Axl$^+$DCs, inducing the activation of STING and the development of a type I IFN response. Of interest, STING can interact with RIG-I and be activated following RIG-I sensing of viral RNA.[42] These findings are in line with our Axl$^+$DC RNA-seq results that show RIG-I implication in HIV-1 sensing (Figure 1). Alternatively, sensing of incoming viral particles at the plasma membrane may trigger an ISG response as previously demonstrated in macrophages,[43] via a cGAS-independent STING-dependent pathway as previously proposed.[44,45]

Looking at DCs isolated from an HIV-1-infected individual during primo-infection, we could not detect HIV-1 transcripts, probably because of the low levels of HIV-1 transcripts present and/or intrinsic limitation of the scRNA-seq technology used. Similar negative results were obtained when analyzing by single-cell transcriptomic PBMCs from four patients during hyperacute or acute HIV-1 infection.[32] Axl$^+$DCs may also escape detection by migrating to lymphoid tissues because HIV-1 exposure induces their CCR7 expression at the mRNA and protein levels (Figures 2E and S4C). Notably, higher levels of CCR7 expression were observed in Axl$^+$DCs experiencing active HIV-1 replication (Figure S4). Therefore, such migrating Axl$^+$DCs could participate in the replication and spread of HIV-1 in the lymphoid organs, where high viral replication occurs in infected patients.[46] Nevertheless, circulating DCs from the patient exhibited transcriptional responses overlapping those we observed *in vitro*. It remains to be determined whether the IFN and NF-kB signaling we measured is a consequence of HIV-1 sensing or the inflammation associated with HIV-1 replication during primo-infection.[47]

Axl$^+$DCs specifically express Siglec-1, which endows them with a high capacity to capture HIV-1, get infected, produce infectious viruses in apparently internal compartments, and transmit the virus to activated T lymphocytes.[24] Although Axl$^+$DCs have been found in various tissues, it remains unclear whether they are also present in mucosal tissues. Of interest, Siglec-1 is also expressed by cervical DCs in the mucosal tissue where HIV-1 transmission occurs.[25,26] Here, we show Axl$^+$DCs have a unique capacity to respond to HIV-1 and promote T cell activation. Future studies using mucosal DCs are granted to estimate whether these different responses to HIV-1 exposure occur *in vivo*. Our results reveal that the distinct sensing pathways activated by HIV-1 in Axl$^+$DCs instruct different outcomes of the innate immune cellular response, which may impact, in turn on HIV-1 viral cycle.

Limitations of the study

The paucity of the Axl$^+$DC population in the blood (less than 1% of the DCs, which represent roughly 1% of the PBMCs) prevented several experiments, including biochemical ones. Genetic manipulations such as gene editing or transgene expression were not achievable in Axl$^+$DCs and thus prevented, for instance, editing STING to demonstrate its involvement in sensing HIV-1. Access to fresh and large blood samples from primo-infected patients was impossible, preventing us from concluding about the physiopathology relevance of our *ex vivo* results. Despite those limitations, our study provides novel, sound, and cross-validated results on the complex role of DCs during HIV-1 infection.

STAR★METHODS

Detailed methods are provided in the online version of this paper and include the following:

- KEY RESOURCES TABLE
- RESOURCE AVAILABILITY
  - Lead contact
  - Materials availability
  - Data and code availability
- EXPERIMENTAL MODEL AND SUBJECT DETAILS
  - Human subjects
  - Human cell lines
  - Primary human cells
- METHOD DETAILS
  - HIV-1 production and titration

- HIV infection of DCs and stimulations
- Bulk RNA sequencing analysis
- Bulk RNA-seq HIV-1 transcripts alignment + CD11c
- Single-cell RNA-Seq library preparation and sequencing
- Single-cell RNA-seq analysis – Read alignment and cell calling
- Single-cell RNAseq analysis – Cell filtering, clustering, and differential expression analysis
- Single-cell RNAseq analysis – Gene network inference
- Single-cell RNAseq analysis – cell labelling
- Single-cell RNA-seq analysis – Quantification of viral infection
- $CD4^+$T cell activation by DCs
- Real-time quantitative PCR
- Cytokine quantification assay by CBA
- Flow Cytometry analyses of DCs from HIV-1 infected patients

● QUANTIFICATION AND STATISTICAL ANALYSIS

- Illustrations

SUPPLEMENTAL INFORMATION

Supplemental information can be found online at https://doi.org/10.1016/j.isci.2023.106019.

ACKNOWLEDGMENTS

We acknowledge the patients for their blood donation. We thank Nicolas Manel at Institut Curie for fruitful discussions, reagents, and critical reading of the manuscript. We also thank Ana-Maria Lennon-Dumenil, François-Xavier Gobert, Julie Helft, Claire Hivroz, Héloïse Delagreverie, Thimothé Bruel, Olivier Schwartz and Sebastian Amigorena for discussions or technical help. We acknowledge NGS curie, the flow cytometry facilities at Institut Curie and Institut Cochin ("plateforme Cytométrie et Immunobiologie"; CYBIO). This work was supported by grants from Agence Nationale de Recherche contre le SIDA et les hépatites virales (ANRS), Ensemble contre le SIDA (Sidaction), Laboratoire d'Excellence (Labex) DCBIOL (ANR-10-IDEX-0001-02 PSL and ANR-11-LABX-0043) to P.B., and Singapore Immunology Network (SIgN) core funding to F.G. Our work also benefitted from France-BioImaging, ANR-10-INSB-04, and Celtisphybio Labex (ANR-10-LBX-0038) part of the Initiative D'EXcellence (Idex) PSL (ANR-10-IDEX-0001-02 PSL). N.R. and F.B. were supported by fellowships from ANRS, Sidaction, and Fondation pour la Recherche Médicale.

AUTHOR CONTRIBUTIONS

N.R. and P.B designed the study. N.R. and F.B performed experiments and analyzed data. F.N. designed and supervised the bioinformatic analyses that were then completed by O.A.M, P.E., and F.B. C.D. and J-D.L. provided clinical samples from HIV-1 infected patients. N.R. and P.B wrote the manuscript with the help of F.B., F.N., and F.G.

DECLARATION OF INTERESTS

All authors declare no conflict of interests.

Received: June 15, 2022
Revised: November 5, 2022
Accepted: January 17, 2023
Published: February 17, 2023

REFERENCES

1. Schlitzer, A., McGovern, N., and Ginhoux, F. (2015). Dendritic cells and monocyte-derived cells: two complementary and integrated functional systems. Semin. Cell Dev. Biol. *41*, 9–22. https://doi.org/10.1016/j.semcdb.2015.03.011.

2. Martín-Moreno, A., and Muñoz-Fernández, M.A. (2019). Dendritic cells, the double agent in the war against hiv-1. Front. Immunol. *10*, 2485. https://doi.org/10.3389/fimmu.2019.02485.

3. Vine, E.E., Rhodes, J.W., Warner van Dijk, F.A., Byrne, S.N., Bertram, K.M., Cunningham, A.L., and Harman, A.N. (2022). HIV transmitting mononuclear phagocytes; integrating the old and new. Mucosal Immunol. *15*, 542–550. https://doi.org/10.1038/S41385-022-00492-0.

4. Hu, Q., Frank, I., Williams, V., Santos, J.J., Watts, P., Griffin, G.E., Moore, J.P., Pope, M., and Shattock, R.J. (2004). Blockade of attachment and fusion receptors inhibits HIV-1 infection of human cervical tissue. J. Exp. Med. *199*, 1065–1075. https://doi.org/10.1084/JEM.20022212.

5. Nasr, N., Lai, J., Botting, R.A., Mercier, S.K., Harman, A.N., Kim, M., Turville, S., Center, R.J., Domagala, T., Gorry, P.R., et al. (2014). Inhibition of two temporal phases of HIV-1 transfer from primary Langerhans cells to T cells: the role of langerin. J. Immunol. *193*, 2554–2564. https://doi.org/10.4049/JIMMUNOL.1400630/-/DCSUPPLEMENTAL.

6. Trifonova, R.T., Bollman, B., Barteneva, N.S., and Lieberman, J. (2018). Myeloid cells in intact human cervical explants capture HIV and can transmit it to CD4 T cells. Front. Immunol. *9*, 2719. https://doi.org/10.3389/FIMMU.2018.02719/BIBTEX.

7. Yin, X., Langer, S., Zhang, Z., Herbert, K.M., Yoh, S., König, R., and Chanda, S.K. (2020). Sensor sensibility—HIV-1 and the innate immune response. Cells *9*, 254. https://doi.org/10.3390/cells9010254.

8. Beignon, A.-S., McKenna, K., Skoberne, M., Manches, O., DaSilva, I., Kavanagh, D.G., Larsson, M., Gorelick, R.J., Lifson, J.D., and Bhardwaj, N. (2005). Endocytosis of HIV-1 activates plasmacytoid dendritic cells via Toll-like receptor-viral RNA interactions. J. Clin. Invest. *115*, 3265–3275. https://doi.org/10.1172/JCI26032.

9. Fonteneau, J.-F., Larsson, M., Beignon, A.-S., McKenna, K., Dasilva, I., Amara, A., Liu, Y.-J., Lifson, J.D., Littman, D.R., and Bhardwaj, N. (2004). Human immunodeficiency virus type 1 activates plasmacytoid dendritic cells and concomitantly induces the bystander maturation of myeloid dendritic cells. J. Virol. *78*, 5223–5232. https://doi.org/10.1128/jvi.78.10.5223-5232.2004.

10. Gringhuis, S.I., van der Vlist, M., van den Berg, L.M., den Dunnen, J., Litjens, M., and Geijtenbeek, T.B.H. (2010). HIV-1 exploits innate signaling by TLR8 and DC-SIGN for productive infection of dendritic cells. Nat. Immunol. *11*, 419–426. https://doi.org/10.1038/ni.1858.

11. Silvin, A., Yu, C.I., Lahaye, X., Imperatore, F., Brault, J.-B., Cardinaud, S., Becker, C., Kwan, W.-H., Conrad, C., Maurin, M., et al. (2017). Constitutive resistance to viral infection in human CD141 $^{+}$ dendritic cells. Sci. Immunol. *2*, eaai8071. https://doi.org/10.1126/sciimmunol.aai8071.

12. Manel, N., Hogstad, B., Wang, Y., Levy, D.E., Unutmaz, D., and Littman, D.R. (2010). A cryptic sensor for HIV-1 activates antiviral innate immunity in dendritic cells. Nature *467*, 214–217. https://doi.org/10.1038/nature09337.

13. Cribier, A., Descours, B., Valadão, A.L.C., Laguette, N., and Benkirane, M. (2013). Phosphorylation of SAMHD1 by cyclin A2/CDK1 regulates its restriction activity toward HIV-1. Cell Rep. *3*, 1036–1043. https://doi.org/10.1016/j.celrep.2013.03.017.

14. Hrecka, K., Hao, C., Gierszewska, M., Swanson, S.K., Kesik-Brodacka, M., Srivastava, S., Florens, L., Washburn, M.P., and Skowronski, J. (2011). Vpx relieves inhibition of HIV-1 infection of macrophages mediated by the SAMHD1 protein. Nature *474*, 658–661. https://doi.org/10.1038/nature10195.

15. Laguette, N., Sobhian, B., Casartelli, N., Ringeard, M., Chable-Bessia, C., Ségéral, E., Yatim, A., Emiliani, S., Schwartz, O., and Benkirane, M. (2011). SAMHD1 is the dendritic- and myeloid-cell-specific HIV-1 restriction factor counteracted by Vpx. Nature *474*, 654–657. https://doi.org/10.1038/nature10117.

16. Lahouassa, H., Daddacha, W., Hofmann, H., Ayinde, D., Logue, E.C., Dragin, L., Bloch, N., Maudet, C., Bertrand, M., Gramberg, T., et al. (2012). SAMHD1 restricts the replication of human immunodeficiency virus type 1 by depleting the intracellular pool of deoxynucleoside triphosphates. Nat. Immunol. *13*, 223–228. https://doi.org/10.1038/ni.2236.

17. Su, B., Biedma, M.E., Lederle, A., Peressin, M., Lambotin, M., Proust, A., Decoville, T., Schmidt, S., Laumond, G., and Moog, C. (2014). Dendritic cell-lymphocyte cross talk downregulates host restriction factor SAMHD1 and stimulates HIV-1 replication in dendritic cells. J. Virol. *88*, 5109–5121. https://doi.org/10.1128/JVI.03057-13.

18. Johnson, J.S., Lucas, S.Y., Amon, L.M., Skelton, S., Nazitto, R., Carbonetti, S., Sather, D.N., Littman, D.R., and Aderem, A. (2018). Reshaping of the dendritic cell chromatin landscape and interferon pathways during HIV infection. Cell Host Microbe *23*, 366–381.e9. https://doi.org/10.1016/j.chom.2018.01.012.

19. Lahaye, X., Satoh, T., Gentili, M., Cerboni, S., Conrad, C., Hurbain, I., El Marjou, A., Lacabaratz, C., Lelièvre, J.D., and Manel, N. (2013). The capsids of HIV-1 and HIV-2 determine immune detection of the viral cDNA by the innate sensor cGAS in dendritic cells. Immunity *39*, 1132–1142. https://doi.org/10.1016/j.immuni.2013.11.002.

20. See, P., Dutertre, C.-A., Chen, J., Günther, P., McGovern, N., Irac, S.E., Gunawan, M., Beyer, M., Händler, K., Duan, K., et al. (2017). Mapping the human DC lineage through the integration of high-dimensional techniques. Science *356*, eaag3009. https://doi.org/10.1126/science.aag3009.

21. Villani, A.-C., Satija, R., Reynolds, G., Sarkizova, S., Shekhar, K., Fletcher, J., Griesbeck, M., Butler, A., Zheng, S., Lazo, S., et al. (2017). Single-cell RNA-seq reveals new types of human blood dendritic cells, monocytes, and progenitors. Science *356*, eaah4573. https://doi.org/10.1126/science.aah4573.

22. Alcántara-Hernández, M., Leylek, R., Wagar, L.E., Engleman, E.G., Keler, T., Marinkovich, M.P., Davis, M.M., Nolan, G.P., and Idoyaga, J. (2017). High-Dimensional phenotypic mapping of human dendritic cells reveals interindividual variation and tissue specialization. Immunity *47*, 1037–1050.e6. https://doi.org/10.1016/j.immuni.2017.11.001.

23. Leylek, R., Alcántara-Hernández, M., Lanzar, Z., Lüdtke, A., Perez, O.A., Reizis, B., and Idoyaga, J. (2019). Integrated cross-species analysis identifies a conserved transitional dendritic cell population. Cell Rep. *29*, 3736–3750.e8. https://doi.org/10.1016/j.celrep.2019.11.042.

24. Ruffin, N., Gea-Mallorquí, E., Brouiller, F., Jouve, M., Silvin, A., See, P., Dutertre, C.-A., Ginhoux, F., and Benaroch, P. (2019). Constitutive Siglec-1 expression confers susceptibility to HIV-1 infection of human dendritic cell precursors. Proc. Natl. Acad. Sci. USA. *116*, 21685–21693.

25. Perez-Zsolt, D., Cantero-Pérez, J., Erkizia, I., Benet, S., Pino, M., Serra-Peinado, C., Hernández-Gallego, A., Castellví, J., Tapia, G., Arnau-Saz, V., et al. (2019). Dendritic cells from the cervical mucosa capture and transfer HIV-1 via siglec-1. Front. Immunol. *10*, 825. https://doi.org/10.3389/FIMMU.2019.00825/BIBTEX.

26. Rhodes, J.W., Botting, R.A., Bertram, K.M., Vine, E.E., Rana, H., Baharlou, H., Vegh, P., O'Neil, T.R., Ashhurst, A.S., Fletcher, J., et al. (2021). Human anogenital monocyte-derived dendritic cells and langerin+cDC2 are major HIV target cells. Nat. Commun. *121*, 2147–2215. https://doi.org/10.1038/s41467-021-22375-x.

27. Izquierdo-Useros, N., Lorizate, M., McLaren, P.J., Telenti, A., Kräusslich, H.G., and Martinez-Picado, J. (2014). HIV-1 capture and transmission by dendritic cells: the role of viral glycolipids and the cellular receptor siglec-1. PLoS Pathog. *10*, e1004146. https://doi.org/10.1371/journal.ppat.1004146.

28. Loré, K., Smed-Sörensen, A., Vasudevan, J., Mascola, J.R., and Koup, R.A. (2005). Myeloid and plasmacytoid dendritic cells transfer HIV-1 preferentially to antigen-specific CD4+ T cells. J. Exp. Med. *201*, 2023–2033. https://doi.org/10.1084/JEM.20042413.

29. Lahaye, X., Gentili, M., Silvin, A., Conrad, C., Picard, L., Jouve, M., Zueva, E., Maurin, M., Nadalin, F., Knott, G.J., et al. (2018). NONO detects the nuclear HIV capsid to promote cGAS-mediated innate immune activation. Cell *175*, 488–501.e22. https://doi.org/10.1016/j.cell.2018.08.062.

30. Rhodes, J.W., Tong, O., Harman, A.N., and Turville, S.G. (2019). Human dendritic cell subsets, ontogeny, and impact on HIV infection. Front. Immunol. *10*, 1088. https://doi.org/10.3389/fimmu.2019.01088.

31. Sáez-Cirión, A., and Manel, N. (2018). Immune responses to retroviruses. Annu. Rev. Immunol. *36*, 193–220. https://doi.org/10.1146/annurev-immunol-051116-052155.

32. Kazer, S.W., Aicher, T.P., Muema, D.M., Carroll, S.L., Ordovas-Montanes, J., Miao, V.N., Tu, A.A., Ziegler, C.G.K., Nyquist, S.K., Wong, E.B., et al. (2020). Integrated single-cell analysis of multicellular immune dynamics during hyperacute HIV-1 infection. Nat. Med. *26*, 511–518. https://doi.org/10.1038/s41591-020-0799-2.

33. Kane, M., Zang, T.M., Rihn, S.J., Zhang, F., Kueck, T., Alim, M., Schoggins, J., Rice, C.M., Wilson, S.J., and Bieniasz, P.D. (2016). Identification of interferon-stimulated genes with antiretroviral activity. Cell Host Microbe *20*, 392–405. https://doi.org/10.1016/j.chom.2016.08.005.

34. Aibar, S., González-Blas, C.B., Moerman, T., Huynh-Thu, V.A., Imrichova, H., Hulselmans, G., Rambow, F., Marine, J.C., Geurts, P., Aerts, J., et al. (2017). SCENIC: single-cell regulatory network inference and clustering. Nat. Methods *14*, 1083–1086.

35. Kiselev, V.Y., Yiu, A., and Hemberg, M. (2018). scmap: projection of single-cell RNA-seq data across data sets. Nat. Methods *15*, 359–362. https://doi.org/10.1038/nmeth.4644.

36. Lahaye, X., and Manel, N. (2015). Viral and cellular mechanisms of the innate immune sensing of HIV. Curr. Opin. Virol. *11*, 55–62. https://doi.org/10.1016/j.coviro.2015.01.013.

37. Choi, Y., Lafferty, J.A., Clements, J.R., Todd, J.K., Gelfand, E.W., Kappler, J., Marrack, P., and Kotzin, B.L. (1990). Selective expansion of T cells expressing V beta 2 in toxic shock syndrome. J. Exp. Med. *172*, 981–984. https://doi.org/10.1084/jem.172.3.981.

38. Johnson, J.S., De Veaux, N., Rives, A.W., Lahaye, X., Lucas, S.Y., Perot, B.P., Luka, M., Garcia-Paredes, V., Amon, L.M., Watters, A., et al. (2020). A comprehensive map of the monocyte-derived dendritic cell transcriptional network engaged upon innate sensing of HIV. Cell Rep. *30*, 914–931.e9. https://doi.org/10.1016/j.celrep.2019.12.054.

39. Abe, T., and Barber, G.N. (2014). Cytosolic-DNA-mediated, STING-dependent proinflammatory gene induction necessitates canonical NF-κB activation through TBK1. J. Virol. *88*, 5328–5341. https://doi.org/10.1128/jvi.00037-14.

40. Hou, Y., Liang, H., Rao, E., Zheng, W., Huang, X., Deng, L., Zhang, Y., Yu, X., Xu, M., Mauceri, H., et al. (2018). Non-canonical NF-κB antagonizes STING sensor-mediated DNA sensing in radiotherapy. Immunity *49*, 490–503.e4. https://doi.org/10.1016/j.immuni.2018.07.008.

41. Alculumbre, S.G., Saint-André, V., Di Domizio, J., Vargas, P., Sirven, P., Bost, P., Maurin, M., Maiuri, P., Wery, M., Roman, M.S., et al. (2018). Diversification of human plasmacytoid predendritic cells in response to a single stimulus. Nat. Immunol. *19*, 63–75. https://doi.org/10.1038/s41590-017-0012-z.

42. Solis, M., Nakhaei, P., Jalalirad, M., Lacoste, J., Douville, R., Arguello, M., Zhao, T., Laughrea, M., Wainberg, M.A., and Hiscott, J. (2011). RIG-I-Mediated antiviral signaling is inhibited in HIV-1 infection by a protease-mediated sequestration of RIG-I. J. Virol. *85*, 1224–1236. https://doi.org/10.1128/JVI.01635-10.

43. Decalf, J., Desdouits, M., Rodrigues, V., Gobert, F.-X., Gentili, M., Marques-Ladeira, S., Chamontin, C., Mougel, M., Cunha de Alencar, B., and Benaroch, P. (2017). Sensing of HIV-1 entry triggers a type I interferon response in human primary macrophages. J. Virol. *91*, e00147–e00217. https://doi.org/10.1128/JVI.00147-17.

44. Holm, C.K., Rahbek, S.H., Gad, H.H., Bak, R.O., Jakobsen, M.R., Jiang, Z., Hansen, A.L., Jensen, S.K., Sun, C., Thomsen, M.K., et al. (2016). Influenza A virus targets a cGAS-independent STING pathway that controls enveloped RNA viruses. Nat. Commun. *7*, 10680. https://doi.org/10.1038/ncomms10680.

45. Jakobsen, M.R., Bak, R.O., Andersen, A., Berg, R.K., Jensen, S.B., Tengchuan, J., Laustsen, A., Hansen, K., Østergaard, L., Fitzgerald, K.A., et al. (2013). IFI16 senses DNA forms of the lentiviral replication cycle and controls HIV-1 replication. Proc. Natl. Acad. Sci. USA. *110*, E4571–E4580. https://doi.org/10.1073/pnas.1311669110.

46. Pantaleo, G., Graziosi, C., and Fauci, A.S. (1993). The role of lymphoid organs in the pathogenesis of HIV infection. Semin. Immunol. *5*, 157–163. https://doi.org/10.1006/SMIM.1993.1019.

47. Kazer, S.W., Walker, B.D., and Shalek, A.K. (2020). Evolution and diversity of immune responses during acute HIV infection. Immunity *53*, 908–924. https://doi.org/10.1016/J.IMMUNI.2020.10.015.

48. Mörner, A., Björndal, A., Albert, J., KewalRamani, V.N., Littman, D.R., Inoue, R., Thorstensson, R., Fenyö, E.M., and Björling, E. (1999). Primary human immunodeficiency virus type 2 (HIV-2) isolates, like HIV-1 isolates, frequently use CCR5 but show promiscuity in coreceptor usage. J. Virol. *73*, 2343–2349. https://doi.org/10.1128/JVI.73.3.2343-2349.1999.

49. Love, M.I., Huber, W., and Anders, S. (2014). Moderated estimation of fold change and dispersion for RNA-seq data with DESeq2. Genome Biol. *15*, 550–571. https://doi.org/10.1186/s13059-014-0550-8.

50. Gu, Z., Eils, R., and Schlesner, M. (2016). Complex heatmaps reveal patterns and correlations in multidimensional genomic data. Bioinformatics *32*, 2847–2849. https://doi.org/10.1093/bioinformatics/btw313.

51. Wickham, H. (2016). ggplot2, Elegant Graphics for Data Analysis (Springer Cham). https://doi.org/10.1007/978-3-319-24277-4.

52. Dobin, A., Davis, C.A., Schlesinger, F., Drenkow, J., Zaleski, C., Jha, S., Batut, P., Chaisson, M., and Gingeras, T.R. (2013). STAR: ultrafast universal RNA-seq aligner. Bioinformatics *29*, 15–21. https://doi.org/10.1093/bioinformatics/bts635.

53. Liao, Y., Smyth, G.K., and Shi, W. (2013). The Subread aligner: fast, accurate and scalable read mapping by seed-and-vote. Nucleic Acids Res. *41*, e108. https://doi.org/10.1093/nar/gkt214.

54. Satija, R., Farrell, J.A., Gennert, D., Schier, A.F., and Regev, A. (2015). Spatial reconstruction of single-cell gene expression data. Nat. Biotechnol. *33*, 495–502.

55. Benaglia, T., Chauveau, D., Hunter, D., and Young, D. (2009). Mixtools: An R Package for Analyzing Finite Mixture Models.

56. Waltman, L., and Van Eck, N.J. (2013). A smart local moving algorithm for large-scale modularity-based community detection. Eur. Phys. J. B *86*, 471. https://doi.org/10.1140/epjb/e2013-40829-0.

57. McInnes, L., Healy, J., Saul, N., and Großberger, L. (2018). UMAP: uniform manifold approximation and projection. J. Open Source Softw. *3*, 861. https://doi.org/10.21105/joss.00861.

58. Freed, E.O., Englund, G., and Martin, M.A. (1995). Role of the basic domain of human immunodeficiency virus type 1 matrix in macrophage infection. J. Virol. *69*, 3949–3954. https://doi.org/10.1128/jvi.69.6.3949-3954.1995.

59. Ritchie, M.E., Phipson, B., Wu, D., Hu, Y., Law, C.W., Shi, W., and Smyth, G.K. (2015). Limma powers differential expression analyses for RNA-sequencing and microarray studies. Nucleic Acids Res. *43*, e47. https://doi.org/10.1093/NAR/GKV007.

60. Zhu, A., Ibrahim, J.G., and Love, M.I. (2019). Heavy-tailed prior distributions for sequence count data: removing the noise and preserving large differences. Bioinformatics *35*, 2084–2092. https://doi.org/10.1093/BIOINFORMATICS/BTY895.

61. Yu, G., Wang, L.G., Han, Y., and He, Q.Y. (2012). clusterProfiler: an R Package for comparing biological themes among gene clusters. OMICS *16*, 284–287. https://doi.org/10.1089/OMI.2011.0118.

STAR★METHODS

KEY RESOURCES TABLE

REAGENT or RESOURCE	SOURCE	IDENTIFIER
Antibodies		
HLA-DR Monoclonal Antibody (LN3), APC-eFluor 780, eBioscience™	Thermo Fisher Scientific	Cat# 47-9956-42; RRID: AB_1963603
CD1c Monoclonal Antibody (L161), PerCP-eFluor 710, eBioscience™	Thermo Fisher Scientific	Cat# 46-0015-42, RRID:AB_10548936
CD123 Antibody, anti-human, VioGreen™, REAfinity™	Miltenyi Biotec	Cat# 130-115-271, RRID:AB_2726974
CD45RA Antibody, anti-human, VioBlue®	Miltenyi Biotec	Cat# 130-113-360, RRID:AB_2726132
PE Anti-human CD370 (Clec9A) antibody	BD Biosciences	Cat# 563488, RRID:AB_2738237
PE-CF594 Mouse Anti-Human CD33 Antibody	BD Biosciences	Cat# 562492, RRID:AB_2713912
Human Axl PE-conjugated Antibody	R&D Systems	Cat# FAP514P; RRID:AB_2894899
Mouse Anti-Human CD19 Monoclonal Antibody, FITC Conjugated Clone LT19	Miltenyi Biotec	Cat# 130-091-328, RRID:AB_244222
Mouse Anti-CD3 Monoclonal Antibody, FITC Conjugated, Clone HIT3a	BD Biosciences	Cat# 555339, RRID:AB_395745
Mouse Anti-CD14 Monoclonal Antibody, FITC Conjugated, Clone M5E2	BD Biosciences	Cat# 555397, RRID:AB_395798
CD16 FITC CE antibody	BD Biosciences	Cat# 335035, RRID:AB_2868680
Mouse Anti-CD34 Monoclonal Antibody, FITC Conjugated, Clone 581	BD Biosciences	Cat# 555821, RRID:AB_396150
HIV-1 core antigen-RD1 antibody	Beckman Coulter	Cat# 6604667, RRID:AB_1575989
Mouse Anti-CD86 Monoclonal Antibody, FITC Conjugated, Clone 2331 (FUN-1)	BD Biosciences	Cat# 555657, RRID:AB_396012
MX1 antibody human, monkey, human, non-human primate	Abcam	Cat# ab95926, RRID:AB_10677452
F(ab')2-Goat anti-Rabbit IgG (H+L) Cross-Adsorbed Secondary Antibody, Alexa Fluor 647	Thermo Fisher Scientific	Cat# A-21246, RRID:AB_2535814
CD11c PE-Cy7	Biolegend	Cat# 337215, RRID:AB_2129791
CD3 AF647	BD Biosciences	Cat# 557706, RRID: AB_396815
CD25 PE	BD Biosciences	Cat# 555432, RRID: AB_395826
BV711 Mouse Anti-Human CD141 Clone 1A4	BD Biosciences	Cat# 563155, RRID: AB_2738033
CD169 (Siglec-1) Antibody, anti-human, PE-Vio770 Clone 7-239	Miltenyi Biotec	Cat# 130-098-640, RRID: AB_2655549
APC-R700 Rat Anti-Human CCR7 (CD197) Clone 3D12	BD Biosciences	Cat# 565867, RRID: AB_2744304
Bacterial and virus strains		
HIV-1(NL-AD8)	Manel et al., 2010[12]	Wildtype HIV-1 molecular clone
Biological samples		
Human Healthyblood donors for primary PBMCs	This manuscript	N/A
Human HIV-1 infected donors for primary PBMCs	This manuscript	N/A
Chemicals, peptides, and recombinant proteins		
TransIT-293 Transfection Reagent	Euromedex	Cat# MIR270
Penicillin-Streptomycin	Thermo Fisher Scientific	Cat# 15140122
Ficoll-Paque PLUS	Dutscher	Cat# 17-1440-03

(*Continued on next page*)

Continued

REAGENT or RESOURCE	SOURCE	IDENTIFIER
Gentamicin (50mg/ml)	Thermo Fisher Scientific	Cat# 15750037
RPMI 1640 Medium, GlutaMAX supplement	Thermo Fisher Scientific	Cat# 61870010
Azidothymidine	SIGMA	Cat# A2169;CAS: 30516-87-1; AZT
Nevirapine	SIGMA	Cat# SML0097;CAS: 129618-40-2; NV
Saponin from quillaja bark	Sigma Aldrich	Cat# S7900-100G
H-151 STING antagonist	Probechem	Cat# HY-112693; CAS: 941987-60-6
CpG-A ODN2216	Invivogen	Cat# tlrl-2216
CL264	Invivogen	Cat# tlrl-c264e
R848	Invivogen	Cat# tlrl-r848 CAS: 144875-48-9
NP40 substitute (IGEPAL CA-630)	Euromedex	Cat# UN3500-A; CAS: 9036-19-5
Paraformaldehyde	Electron Microscopy Sciences	Cat# 15710; CAS: 30525-89-4
CFSE	Invitrogen	Cat# C34570
rTSST1	Toxin Technology	Cat# rTT606
Live/Dead Near-IR Red stain	Life technologies	Cat# L34975
Critical commercial assays		
EasySep human pan-DC pre-enrichment kit	Stemcell Technologies	Cat# 19251
naïve $CD4^+$T Cell Isolation Kit	Miltenyi Biotec	Cat# 130-094-131
Human IP-10 Flex Set	BD	Cat# 558280
Human MIP-1a Flex Set	BD	Cat# 558325
Human IL-8 Flex Set	BD	Cat# 558277
Human IL-2 Flex Set	BD	Cat# 558270
Single Cell RNA purification Kit	NORGEN	Cat# 51800
RNA 6000 pico Kit	Agilent	Cat# 5067-1513
SMART-Seq v4 ultraLow Input RNA kit	Takara Bio	Cat# 634891
Qubit dsDNA HS Assay kit	Invitrogen	Cat# Q322851
KAPA HyperPlus Kits	ROCHE	Cat# 07962428001
Chromium Single Cell 3' v2 Reagent Kit	10X Genomics	Cat# 120234
RNeasy micro kit	Qiagen	Cat# 740004
high-capacity cDNA reverse transcription kit	Applied Biosystems	Cat# 4374966
LightCycler® 480 SYBR Green I Master	Roche	Cat# 04707516001
Deposited data		
Raw and analysed data	This manuscript	NCBI GEO: GSE189748 Go to https://www.ncbi.nlm.nih.gov/geo/query/acc.cgi?acc=GSE189748
Analyses scripts	This manuscript	https://github.com/pbenaroch-lab/preDCxHIV1
human GRCh38 genome	https://www.ncbi.nlm.nih.gov/genbank/	GenBank accession: GCA_000001405.25
HIV-1 reference genome	https://www.ncbi.nlm.nih.gov	GenBank accession: NC_001802
HIV-1 genome sequence containing the HIV-2 protein sequence vpx	https://www.ncbi.nlm.nih.gov	GenBank accession: NC_001802.1
Experimental models: Cell lines		
293FT	Thermo Fisher Scientific	Cat# R70007, RRID: CVCL_6911
GHOSTX4R5	Mörner et al., 1999[48]	https://doi.org/10.1128/JVI.73.3.2343-2349.1999

(*Continued on next page*)

Continued

REAGENT or RESOURCE	SOURCE	IDENTIFIER
Oligonucleotides		
MX1	Eurogentec	F : 5′-AGCTCGGCAACAGACTCTTC-3′ R: 5′- GATGATAAAGGGATGTGGC-3′
IFNB	Eurogentec	F : 5′-CCTGTGGCAATTGAATGGGAGGC-3′ R: 5′-CCAGGCACAGTGACTGTACTCCTT-3′
RSP18	Eurogentec	F : 5′-CTGCCATTAAGGGTGTGG-3′ R: 5′-TCAATGTCTGCTTTCCTCAAC-3′
Recombinant DNA		
pNL4.3 AD8	Manel et al.,2010[12]	N/A
pIRES2EGFP-VPXanyVPR	Manel et al.,2010[12]	N/A
Software and algorithms		
GraphPad Prism 7	GraphPad	https://www.graphpad.com/
FlowJo	Tree Star	https://www.flowjo.com
DIVA	BD	https://www.bdbiosciences.com/en-fr/products/software/instrument-software/bd-facsdiva-software#Overview
FCAP Array – Version 3.0.14.1993	BD	http://www.bdbiosciences.com/us/applications/research/bead-based-immunoassays/analysis-software/fcap-array-software-v30/p/652099
The R-project (v 3.5.3 and v 4.2.1)	The R foundation	https://www.r-project.org/
TrimGalore v.0.6.2	Felix Krueger	https://github.com/FelixKrueger/TrimGalore
DEseq2 Package (v1.36.00)	Bioconductor Love et al., 2014[49]	https://bioconductor.org/packages/release/bioc/html/DESeq2.html RRID: SCR_015687
limma Package	Bioconductor	https://bioconductor.org/packages/release/bioc/html/limma.html RRID: SCR_010943
pheatmap Package	R Kolde, 2015	https://cran.r-project.org/web/packages/pheatmap/pheatmap.pdf RRID: SCR_016418
ComplexHeatmap Package, version 2.8.0	Gu et al., 2016[50]	http://bioconductor.org/packages/release/bioc/html/ComplexHeatmap.html RRID: SCR_017270
ggplot Package	Wickham, 2016[51]	https://ggplot2.tidyverse.org/ RRID : SCR_014601
STAR (v2.7.3a)	Dobin et al., 2013[52]	http://code.google.com/p/rna-star/
featureCounts from Subread (v1.5.1)	Liao et al., 2013[53]	https://bioconductor.org/packages/release/bioc/html/Rsubread.html RRID: SCR_009803
Seurat package (V3.1.1)	Satija et al., 201[54]	https://satijalab.org/seurat/ RRID: SCR_016341
SCENIC package v1.1.1-9	Aibar et al., 2017[34]	https://scenic.aertslab.org/ RRID: SCR_017247
Mixtools package v1.1.0	Benaglia et al., 2009[55]	https://cran.r-project.org/web/packages/mixtools/mixtools.pdf
GSEA Software (v4.1.0)	UC San Diego	http://www.broadinstitute.org/gsea/ RRID : SCR_003199

(*Continued on next page*)

Continued

REAGENT or RESOURCE	SOURCE	IDENTIFIER
MSigDB (v7.0)	UC San Diego (GSEA)	http://software.broadinstitute.org/gsea/msigdb/index.jsp RRID: SCR_016863
Cell Ranger Single Cell Software Suite (v2.1.0)	10X Genomics	https://www.10xgenomics.com/
Waltman and van Eck Algorithm	Waltman and van Eck, 2013;[56] McInnes et al., 2018[57]	https://github.com/lmcinnes/umap
Biorender	Biorender	www.biorender.com
Affinity Designer v. 1.10.1.1142	Affinity	https://affinity.serif.com/en-us/
Other		
X-VIVO-15 media	Lonza	Cat# BE04-418F
DMEM medium, GlutaMAX	Thermo Fisher	Cat# 61965-026
AMPure XP Beads	Beckman Coulter	Cat# A63881

RESOURCE AVAILABILITY

Lead contact

Further information and requests for resources and reagents should be directed to and will be fulfilled by the lead contact, Dr Philippe Benaroch (philippe.benaroch@curie.fr).

Materials availability

This study did not generate new unique reagents.

Data and code availability

Bulk and single cell RNAseq data have been deposited at *NCBI* and are publicly available as of the date of publication. Accession numbers are listed in the key resources table.

All original code has been deposited at *Github* and is publicly available as of the date of publication. DOIs are listed in the key resources table.

Any additional information required to reanalyse the data reported in this paper is available from the lead contact upon request.

EXPERIMENTAL MODEL AND SUBJECT DETAILS

Human subjects

Healthy individuals from Paris area donated venous blood to be used for research. Gender identity and age from anonymous healthy donors was not available. According to the 2016 activity report of EFS (French Blood Establishment), half of donors are under 40 years old, and consist of 52% females and 48% males. The use of EFS blood samples from anonymous donor was approved by the *Institut National de la Santé et de la Recherche Médicale* committee. EFS provides informed consent to blood donors. HIV-1 infected individuals (n=32) from Paris area donate venous blood to be used for research. Gender identity, age, HIV-1 viremia and CD4 T cell counts are described in Table S5. The study was approved by ethical committee (*Comité de protection des personnes* CPP, ID-RCB 2017-A02820-53). Written informed consent was obtained from all donors.

Human cell lines

Cell lines are described in the key resources table. Cell lines included 293FT, GHOSTX4R5. 293FT cells were cultured in DMEM medium, GlutaMAX (Thermo Fisher 61965-026) complemented with FBS 10% and Penicillin/Streptomycin. GHOSTX4R5 cells were cultured in DMEM medium, GlutaMAX complemented with FBS 10% and Penicillin/Streptomycin (Thermo Fisher 10378-016). All cells were cultured at 37°C with 5% CO_2 atmosphere. Number of experimental replicates are indicated in the respective figure legends.

Primary human cells

Peripheral blood mononuclear cells (PBMC) were isolated from buffy coats from healthy human donors (approved by the *Institut National de la Santé et de la Recherche Médicale* ethics committee) with Ficoll-Paque PLUS (GE). Informed consent was obtained from all donors, and samples were de-identified prior to use in the study. Total blood DCs were enriched with EasySep human pan-DC pre-enrichment kit (Stemcell Technologies 19251). DC enriched fraction were stained with antibodies specific for HLA-DR APCeFluor780, CD1c PerCPeFluor710 (eBioscience), CD123 Viogreen, CD45RA Vioblue (Miltenyi), Axl PE (Clone #108724, R&D Systems), CD33 PE-CF594, Clec-9A PE (BD) and with a cocktail of antibodies against lineage markers CD19 (Miltenyi), CD3, CD14, CD16 and CD34 (BD) in the FITC channel. Axl^+DCs were sorted as Lin^- $HLADR^+$ $CD33^{int}$ $CD45RA^{int}$ $CD123^+$ Axl^+. pDCs were sorted as Lin^- $HLADR^+$ $CD33^-$ $CD45RA^+$ $CD123^+$ Axl^-. cDC2 were sorted as Lin^- $HLADR^+$ $CD33^+$ $CD45RA^-$ $CD123^-$ $CD1c^+$. cDC1 were sorted as Lin^- $HLADR^+$ $CD33^+$ $CD45RA^-$ $CD123^-$ $Clec9A^+$. For the isolation of $CD11^{hi}$ and $CD11c^{low}$ Axl^+DCs, CD11c APC was added to the antibody cocktail prior to FACS-sorting. All cells were sorted on a FACS Aria (BD) using Diva software (BD) in 5mL polypropylene round-bottom tubes containing 1mL X-VIVO-15 media (Lonza BE04-418F). Post-sort cell purity after gating on live cells by FCS/SSC was routinely between 90 and 99%. DCs were cultured in X-VIVO-15 complemented with Penicillin/Streptomycin.

Naïve $CD4^+$ T cells were isolated from PBMC by negative selection using naïve $CD4^+$T Cell Isolation Kit (Miltenyi 130-094-131) and cultured in RPMI medium 1640, GlutaMAX complemented with FBS 10%, Gentamicin and HEPES. Number of donors and experimental replicates are indicated in the respective figure legends.

METHOD DETAILS

HIV-1 production and titration

Viral particles were produced by transfection of HEK293FT cells in 6-well plates with 3µg DNA and 8µL TransIT-293 (Mirus Bio) per well. For HIV-1(NL-AD8) (described in[58]), 3µg of HIV plasmid were used. For HIV-1(NL-AD8) virus containing Vpx, 0.5µg pIRES2EGFP-VPXanyVPR and 2.5µg HIV plasmid were used. 16h after transfection, media was removed, and fresh X-VIVO-15 was added. Viral supernatants were harvested 36h later, filtered at 0.45µM, aliquoted and frozen at -80°C. Viral titers were determined on GHOST X4R5 cells as described.[48]

HIV infection of DCs and stimulations

Sorted cells were pelleted and resuspended in complete X-VIVO-15 at $0.4*10^6$ cells/mL and 50µL were seeded in round bottom 96-well plates. In some experiments STING antagonist (H-151, Probechem) was added at 20µg/mL and cells incubated for 30 minat 37°C before adding the virus. Azidothymidine (AZT; Sigma) was used at 25 µM final concentration, and nevirapine (NVP; Sigma) was used at 5 µM final concentration. For TLR ligand stimulation, CpG-A (ODN2216, Invivogen) was used at 5µg/mL, R848 (Invivogen) at 10µg/mL. For infections, 150µl of media or dilutions of mock or viral supernatants were added. 48hr after infection, cell culture supernatants were harvested, after neutralisation with 10% NP40 lysis buffer, for IP-10 (CXCL10), MIP1α (CCL3) and IL-8 (CXCL8) quantification using BD CBA Flex Set Kits. Cells were fixed in 4% paraformaldehyde (PFA; Electron Microscopy Sciences) in PBS prior to analysis. Cells were stained with KC57 RD1 (Beckman Coulter 6604667), CD86 FITC (BD 555657), CCR7 APC-R700 (BD 565867) and pure MX1 (abcam ab95926) coupled with a goat anti-rabbit AF647 secondary antibody (Invitrogen A21245) and analysed on a FACS Verse flow cytometer (BD). Data were analysed using FlowJo v10 and Prism v7 for Mac (GraphPad).

For RNA sequencing, after 12h or 24h of culture, cells were harvested and processed with the Chromium Controller (for 10X Genomics single-cell RNA sequencing) or lysed in Lysis buffer from Single Cell RNA purification Kit (NORGEN) for RNA extraction.

Bulk RNA sequencing analysis

Total RNA was isolated from FACS-sorted and HIV-1 infected blood Axl^+DCs, Axl^+ $CD11c^{hi}$ DCs, Axl^+ $CD11c^{lo}$ DCs, pDCs, cDC1 and cDC2 using a Single Cell RNA Purification Kit (Norgen 51800). Total RNA integrity was assessed using an Agilent Bioanalyzer (Agilent RNA 6000 pico Kit 5067-1513) and the RIN and DV200 were calculated. All RNA samples had a RIN >7.0 (except 1 sample at RIN = 6.5). cDNA generation and amplification were performed with SMART-Seq v4 UltraLow Input RNA kit (Takara Bio 634891).

Amplified cDNA was purified using AMPure XP Beads (Beckman Coulter A63881). The concentration of cDNA was determined by Qubit (Invitrogen Qubit dsDNA HS Assay kit Q322851) and LabChip electrophoresis (Perkin Elmer). Libraries were generated using the KAPA HyperPlus Kits (ROCHE) and quantified by Qubit. cDNA libraries were subjected to next generation sequencing using an Illumina NovaSeq6000 instrument.

Sequencing reads were trimmed with TrimGalore v.0.6.2 (https://github.com/FelixKrueger/TrimGalore) to remove adaptors then aligned to the human genome hg38 (v93) with STAR version 2.7.3a.[52]

Differential gene expression analysis was performed with R (v 4.2.1) with the DESeq2 version 1.36.00[49] and the limma Package[59] to remove donor effect. Gene expression levels were analysed on a base-2 logarithmic scale. Shrinkage of log2 fold changes was performed using lfcShrink function from DESeq2 in order to correct imprecise foldchanges and better compare estimated log2 fold changes across experiments.[60] Statistical tests were performed and the p-values were corrected for multiple testing with the Benjamini Hochberg method. Genes with |log2FC| > 1 and an adjusted p-value <0.05 were considered differentially expressed genes (DEG). Heatmaps were produced using R packages pheatmap (https://www.rdocumentation.org/packages/pheatmap/versions/0.2/topics/pheatmap) and ComplexHeatmap[50] (version 2.12.1). GSEA (Gene Set Enrichment Analysis) was performed using the GSEA Software (v4.2.3) and gene signatures from MSigDB (v7.0). GSEA has been performed with the default parameters of GSEAPreranked analysis (number of permutations = 1000 and number of minimum genes = 15). Principal component analysis was performed using R packages DEseq2 and ggplot2 (v 3.3.6).

Pathway analysis was performed on DEG with either GeneOntology term (Biological Processes), KEGG or REACTOME databases from clusterProfiler v4.0.5.[61]

Bulk RNA-seq HIV-1 transcripts alignment + CD11c

100 bp Paired-end RNA-Seq reads were first trimmed with TrimGalore v.0.6.2 (https://github.com/FelixKrueger/TrimGalore) to remove adaptors and mapped onto the hg38 (v93) genome using STAR version 2.7.1a,[52] then the fraction of unmapped reads was mapped on the plasmid sequence (HIV-1 genome sequence (NC_001802.1) containing the HIV-2 protein sequence Vpx) using the STAR version cited above. Chimeric reads were removed after each mapping. Expression levels of individual genes were obtained using featureCounts from Subread[53] version 1.5.1 and TPM were calculated for each gene. Differential expression analysis was performed using DESeq2 version 1.36.0[49] on raw read counts to obtain normalised fold changes (FC) and *Padj*-values for each gene. The analyses scripts are deposited in https://github.com/pbenaroch-lab/preDCxHIV1.

Single-cell RNA-Seq library preparation and sequencing

We performed two distinct scRNAseq analyses. A first experiment (replicate 1) consisted of Axl^{+}DC samples infected for 12 or 24h with HIV-1(NL-AD8)+Vpx with or without AZT treatment, or stimulated for 12 or 24h with CpG-A (TLR9 ligand). A second experiment (replicate 2) refers to Axl^{+}DC samples infected for 24h with HIV-1(NL-AD8) or HIV-1(NL-AD8)+Vpx.

Cellular suspensions of uninfected, HIV-1 infected or TLR9 stimulated Axl^{+}DCs were loaded on a Chromium controller (10X Genomics) according to manufacturer's protocol. scRNASeq libraries were prepared using Chromium Single Cell 3' v2 Reagent Kit (10X Genomics) according to the manufacturer's protocol. Briefly, after performing an emulsion, single cells were trapped into single droplets containing gel beads coated with unique primers bearing 10X barcodes, unique molecular identifier (UMI) and poly(dT) sequences. Reverse transcription reactions were performed in single droplets to produce full-length cDNA. After disruption of emulsion and cDNA clean-up, pooled cDNA were amplified by PCR for 14 cycles to obtain sufficient material used for library preparation using the Chromium Single Cell 3' v2 reagents. Library quantification and quality assessment was performed by LabChip. Indexed libraries were subjected to next generation sequencing using an Illumina HiSeq2500 instrument.

Single-cell RNA-seq analysis – Read alignment and cell calling

Fastq files are obtained from BCF files using mkfastq command from CellRanger v2.1.0. A custom reference genome is created by concatenating the human reference genome GRCh38 (accession: GCA_000001405.25) and the plasmid sequence (pNL4.3 AD8). The annotation from Ensembl v91 is used

for GRCh38. To annotate the plasmid genome, we use the annotation of the HIV-1 reference genome (accession: NC_001802) and mapped gene loci to the plasmid sequence. The final reference is built from protein-coding genes using CellRanger mkgtf and mkref. Reads are aligned to the reference using CellRanger count.

Single-cell RNAseq analysis – Cell filtering, clustering, and differential expression analysis

For replicate 1, filtered gene-cell expression matrices returned by CellRanger count are concatenated to create two merged matrices, respectively containing five (mock and HIV-1 infected) or seven samples (mock, HIV-1 infected, or CpGA exposed), using Seurat v2.3.4.[54] Cells with less than 200 detected genes (UMI count >0) and genes detected in less than 3 cells are filtered out.

For replicate 2, Axl^+DCs are extracted from a DC mock sample by computing the highly variable genes (as above), then the top 20 PCs, and finally the clustering with parameters k=30 and r=0.1, which results in two major clusters. The Axl^+DC population is identified by matching expressed markers (AXL^+, $CD5^+$, and $CX3CR1^+$). The gene-cell matrix for the three Axl^+ samples (mock, HIV-1(NL-AD8), and HIV-1(NL-AD8)+Vpx) are concatenated to obtain a merged matrix and processed as above.

The merged matrices obtained are library-normalised with the formula $\log((10000 \cdot c_g+1)/c_t)$, where c_g is the UMI count for gene g and c_t is the total UMI count in the cell. Highly variable cellular genes (hvg) are computed from the normalised matrices using mean.var.plot method setting the average expression in [0.1, 8] and the scaled dispersion >1. PCA is computed on the scaled hvg-cell matrices and the top n significant PCs (p-value $\leq 10^{-5}$; JackStraw method, default parameters) are selected and projected with Uniform Manifold Approximation and Projection (UMAP) using 30 neighbours and distance cut-off 0.3. Cells are clustered on the n PCs using the Waltman and van Eck algorithm[57,56] with k=30 neighbours and resolution r. [n=22 and r=0.3 for the 5-sample matrix; n=26 and r=0.4 for the 7-sample matrix; a small cluster composed of contaminant cells (38 for the 5-sample matrix, 68 for the 7-sample matrix) was removed from downstream analysis]. Overall, 3021 cells (5-sample) and 3949 cells (7-sample) were retained, respectively.

Differentially expressed genes (DEG) between clusters and between a cluster and its complementary are identified using MAST method. Differentially expressed genes (DEGs) are defined as genes expressed in at least 10% of the cells in either of the two conditions with log2FC > 0.5 and adjusted p-value <0.05 (Bonferroni correction).

Heatmaps and Violin plots were plotted using Seurat. Signature scores were computed using the Seurat "AddModuleScore" and the gene signature of interest. Feature plots were plotted using minimum and maximum cut-off values for each feature respectively quantile 3 and quantile 97.

Single-cell RNAseq analysis – Gene network inference

We used the R package SCENIC v1.1.1-9, which includes three main modules: GENIE3 for network inference from gene expression data, RcisTarget for identification of direct regulatory links, and AUCell for estimating regulon activity on each cell.[34] The input to GENIE3 is a gene-cell expression matrix that has been previously filtered to keep only the genes that are detected in at least 20 cells (UMI count >0). Genes that are co-expressed with a TF are called modules. Note that GENIE3 identifies both positive and negative regulation links.

Spearman rank coefficient is computed for each putative TF-target link and only the positive correlations are retained ($\varrho > 0.3$). The modules are screened with RcisTarget v1.2.1 using the motif-TF annotation, retrieved from hg19-tss-centered-10kb-7species/mc9nr.feather. The output is a set of candidate target genes for each TF. Only the top scoring 10 TF are retained for each target gene. The gene sets obtained are called regulons. Of those, only the ones found in at least 50 out of 100 SCENIC runs computed on uniform random cell subsamples (50% of the cells each) are retained.

An AUCell score is computed for each pair of cell-regulon. The score is computed by first ranking all the genes in a cell according to their expression, and then evaluating the position of the genes in the regulon in the ranked list by AUC. The shape of the distribution obtained was evaluated using the

AUC_exploreThresholds function from the AUCell R package to define a threshold of positive cells where the regulon is active.

SCENIC was run on the two concatenated matrices containing the five (replicate 1) or three samples (replicate 2), respectively, as in "Single-Cell RNAseq analysis – Cell filtering, clustering, and differential expression analysis".

Single-cell RNAseq analysis – cell labelling

Cells for the Axl$^+$ DC samples infected with HIV-1 are mapped onto the four clusters obtained for the first experiments using scmap v1.4.1. The top 500 significantly variable human genes are first selected with a modified version of the M3Drop method on the gene-cell count matrix for experiment 1 containing the cells belonging to the four clusters. For each cell in experiment 2, three correlation values (cosine similarity, Pearson and Spearman) are calculated with respect to each cluster centroid, on the variable genes previously selected. A cell is assigned to a cluster if at least two correlation values are >0.7, otherwise is left unassigned. The result of the mapping is then plotted using plotly v4.8.0.

Single-cell RNA-seq analysis – Quantification of viral infection

The viral UMI fraction per cell is computed as $f = \log_{10}((10000 \cdot c_v+1)/c_t)$, where c_v is the viral UMI count and c_t is the total UMI count (cellular and viral). A normal mixture model for f on the sample exposed to HIV-1(NL-AD8)+Vpx for 24h (replicate 1) is computed, using normalmixEM (default parameters) from R package mixtools v1.1.0.[55] Two distributions are predicted. Cells with $f \geq t$ are defined as productively infected, where t is the maximum between the 99th percentile of the leftmost distribution and the 1st percentile of the rightmost distribution.

Spliced viral transcripts are detected as follows. A read is considered as spliced if it maps with a gap around the tat/rev splicing junction (with a tolerance of 5 bp), unspliced if it maps to an exon and to the contiguous intron (for at least 3 bp), unclassified otherwise. A spliced transcript is defined as a UMI supported by at least 2 reads such that the fraction of spliced reads is $\geq$80% of all classified reads (spliced and unspliced).

CD4$^+$T cell activation by DCs

For each experiment, DC populations and naïve CD4$^+$ T cells were isolated from the same donor. Sorted DCs were pelleted and resuspended in X-VIVO-15 media at 0.4*10^6 cells/mL and 50µL were seeded in round bottom 96-well plates. Dilutions of viral supernatants for MOI of 2 were added up to 150uL and incubated overnight at 37°C. Supernatant was then removed and previously CFSE stained autologous naïve CD4$^+$ T cells were added at a ratio of 1:10 (1 DC for 10 T cells) in the presence of SuperAntigen TSST-1 (0.5 ng/mL). After 48h or 72h of co-culture, supernatants were harvested and neutralised with NP40 10X and cells were fixed in 4% PFA in PBS. Cells were then stained with Live/Dead Near-IR Red stain, CD3 AF647 and CD25 PE (BD) and analysed on a FACS Verse (BD). Supernatants were processed for IL-2 quantification using BD CBA Flex Set Kit. Data were analysed using FlowJo v10 and Prism v7 for Mac (GraphPad).

Real-time quantitative PCR

4*10^5 sorted DC were used *ex-vivo* or treated as described. Cells were lysed, RNA was extracted using RNeasy micro kit (Qiagen) or Single Cell RNA purification Kit (Norgen 51800) and reverse transcription was performed using a high-capacity cDNA reverse transcription kit (Applied Biosystems) by following the manufacturer's instructions. Real-time quantitative PCR was performed using SYBR Green I Master (Roche) with the primers described in the Key resource table (Eurogentec).

The relative quantity of *IFNB1* and *MX1* mRNAs was calculated between *IFNB1* or *MX1* RNA Cp and *RPS18* Cp by the 2-ΔCt method.

Cytokine quantification assay by CBA

IP-10 (CXCL10), MIP1α (CCL3), IL-8 (CXCL8) and IL-2 concentration were measured on non-diluted or 10-fold diluted supernatants using Human cytometric assay from BD according to the manufacturer's protocol. Data was acquired on a FACS Verse (BD) and analysed in FlowJo v10 and GraphPad prism v7 for Mac.

Flow Cytometry analyses of DCs from HIV-1 infected patients

Peripheral blood mononuclear cells (PBMC) were isolated from HIV-1-infected patients (approved by *Comité de protection des personnes* CPP, ID-RCB 2017-A02820-53) or from controls (approved by the *Institut National de la Santé et de la Recherche Médicale* ethics committee) with Ficoll-Paque PLUS (GE). Informed consent was obtained from all donors, and samples were de-identified prior to use in the study. Total blood DCs were enriched with EasySep human pan-DC pre-enrichment kit (Stemcell Technologies 19251). DC enriched fraction were stained with antibodies specific for HLA-DR APCeFluor780, CD1c PerCPeFluor710 (eBioscience), CD123 Viogreen, CD45RA Vioblue, CD169 (Siglec-1) PE-Vio770 (Miltenyi), Axl PE (Clone #108724, R&D Systems), CD33 PE-CF594, CD141 BV711 (BD) and with a cocktail of antibodies against lineage markers CD19 (Miltenyi), CD3, CD14, CD16 and CD34 (BD) in the FITC channel. Data was acquired on a on a FACS Aria using Diva software (BD) and analysed in FlowJo v10 and GraphPad prism v7 for Mac.

QUANTIFICATION AND STATISTICAL ANALYSIS

Flow cytometry and qPCR data were analysed using Prism v7 for Mac (GraphPad). Friedman test was used followed by Dunn's multiple comparisons tests and a p-value lower than 0.05 was considered as significant (*$p<0.05$; **$p<0.01$; ***$p<0.001$ and ****$p<0.0001$).

Illustrations

Figures and Graphical abstract were created using Affinity Designer (version 1.10.1.1142, Affinity) and with BioRender.com respectively.